Grant Agreement No: 101096307

Full Title: THz Industrial Mesh Networks in Smart Sensing and Propagation Environments

Start date: 01/01/2023

End date: 31/03/2026

Duration: 39 Months

Deliverable D6.4

PoC Validation

Document Type	Deliverable
Title	D6.4 – PoC Validation
Contractual due date	31/03/2026
Actual submission date	31/03/2026
Nature	Report
Dissemination Level	Public
Lead Beneficiary	CNRS
Responsible Author	
Contributions from	F. Dutin (CNRS), S. Kroos (TUBS), G. Ducournau (CNRS), F.Meoni (BI-REX), L.Patera (BI-REX), V. Elesina (TUBS)

Revision history

Version	Issue Date	Changes	Contributor(s)
V1.0	15/01/2026	Structure Definition	Francesco Meoni (BI-REX)
V1.1	20/02/2026	PoC2 – industrial validation section	Lorenzo Patera (BI-REX)
V1.2	13/03/2026	PoC2 – Technical Update	Steffen Kroos (TUBS)
V1.3	17/03/2026	PoC2 – industrial validation section 3.2.2	Lorenzo Patera (BI-REX)
V1.4	27/03/2026	PoC1 – Description and Validation	Dutin, G. Ducournau (CNRS)
V1.5	30/3/2026	Review	Kallfass (USTT), Chartier (IAF)
V1.6	31/3/2026	Review Implementation	Meoni, Patera (BI-REX), Kroos, Elesina (TUBS), Ducournau (CNRS)
V2.0	15/4/2026	Final version approved	Luca Sanguinetti (CNIT)

Table of Contents

List of Abbreviations

AoA Angle of Arrival
AoD Angle of Departure
B2B Back-to-back (direct connection with waveguides)
BS Base Station
CINR Carrier to Interference and Noise Ratio (dB)
FDD Frequency Division Duplex
FWG Flexible Waveguide
IDU TIMES Indoor Units (Tx and Rx converters)
IF Intermediate Frequency
LHA Lens Horn Antenna
LNA Low Noise Amplifier
LO Local Oscillator
LoS Line-of-Sight
LWA Leaky-Wave Antenna
MPA Medium Power Amplifier
MS Mobile Station
NLoS Non-Line of Sight
OTA Over the Air
PC Personal Computer
PHY Physical Layer
PLL Phase Locked Loop
PoC Proof of Concept
PoE Power over Ethernet
RF Radio Frequency
RIS Reconfigurable Intelligent Surface
RSSI Received Signal Strength Indicator (dBm)
TDD Time Division Duplex
THz Terahertz
VA Variable Attenuator
VNA Vector Network Analyzer

Executive Summary

This deliverable (D6.4 – PoC Validation) presents the final validation of the TIMES Proofs of Concept (PoCs), focusing on the integration, testing, and industrial assessment. It consolidates previous integration work (notably D6.3) and demonstrates system feasibility in both laboratory and industrial environments.

Two complementary PoCs are validated.

- **PoC-1** demonstrates a RIS-assisted point-to-point THz link in non-line-of-sight conditions, integrating TIMES RF front-ends, antennas, and passive RIS. Validation was performed both in laboratory conditions (~12 m) and in an industrial environment (~40 m). Results confirm stable connectivity with data rates up to 4.15 Gbps (QAM-16) and sub-millisecond latency. The experiments highlight the importance of alignment, link budget optimization, and the feasibility of RIS-enabled THz links for industrial scenarios.
- **PoC-2** focuses on dynamic THz communication with beam-steering capabilities. Two approaches are explored: frequency-controlled steering via leaky-wave antenna (LWA) and RIS-assisted NLoS links. The LWA-based solution demonstrates adaptive beam control through frequency tuning, enabling multi-Gbps throughput and sub-millisecond latency. Industrial validation by BI-REX confirms its relevance for low-latency and high-throughput applications, such as real-time control and high-bandwidth sensing.

The RIS-assisted approach further explores connectivity in obstructed environments, achieving up to ~730 Mbps, while highlighting current limitations in robustness. Nevertheless, it shows strong potential for extending coverage in complex industrial layouts.

Overall, the results confirm the feasibility and industrial potential of THz communications, outperforming conventional wireless technologies in short-range, high-capacity scenarios. The deliverable also identifies key future directions, including improved robustness, autonomous beam management, and enhanced RIS performance, supporting the path toward real-world deployment.

In addition, the deliverable includes, in the Appendix, a dedicated review of the state of knowledge and assessment methodologies for electromagnetic field (EMF) exposure at low-terahertz (low-THz) and terahertz (THz) frequencies. This analysis is motivated by the extension of emerging wireless technologies beyond the 300 GHz range currently covered by established RF-EMF regulatory frameworks. Particular attention is given to the industrial scenarios considered in TIMES, characterized by short communication distances, large-aperture antenna systems, potential worker proximity, dynamic operation, and complex propagation environments. These factors introduce additional challenges for exposure assessment compared to conventional far-field macro-cellular scenarios, and motivate the need for dedicated evaluation approaches.

1 Introduction

1.1 Scope and audience

This deliverable provides a summary of the integration phase for both PoC1 and PoC2. This report is intended for internal use by the TIMES Consortium and for public dissemination

1.2 Structure

The rest of the document is structured as follows:

- Section 2 presents the Proof-of-concept-1, divided into two sub-sections: technical result and industrial validation.
- Section 3 presents the Proof-of-concept-2, divided into two sub-sections: technical result and industrial validation.
- Section 4 contains the list of references.
- The appendix addresses the work done on EMF analysis.

2 PoC-1: Point-to-Point THz Link over RIS

2.1 Context (outcome of D6.3)

For PoC 1, deliverable D6.3 primarily presented the results obtained during back-to-back (B2B) measurements, although it did include an introduction to the final free-space demonstration. We will therefore summarize the key points here.

2.1.1 System Overview

Fig. 1 illustrates the network architecture used in PoC 1. A more detailed description is provided in the following sections; however, this diagram offers an overview of the system. First, the Frequency Division Duplex (FDD) modems interface the network equipment with the front-end modules prior to the up/down conversion to sub-THz frequencies. The front-end modules—composed of integrated circuits on both the transmit and receive (T/R) paths—are connected to the modems. They perform the up/down conversion of the signals and mainly include a local oscillator (LO) with an ×8 frequency multiplier, which is required for operation at sub-THz frequencies. High-gain antennas provide the transition between the waveguide and free-space propagation domains. Finally, the Reflective Intelligent Surface (RIS) establishes the link between the T and R interfaces in a non-line-of-sight (NLoS) propagation channel at sub-THz frequencies.

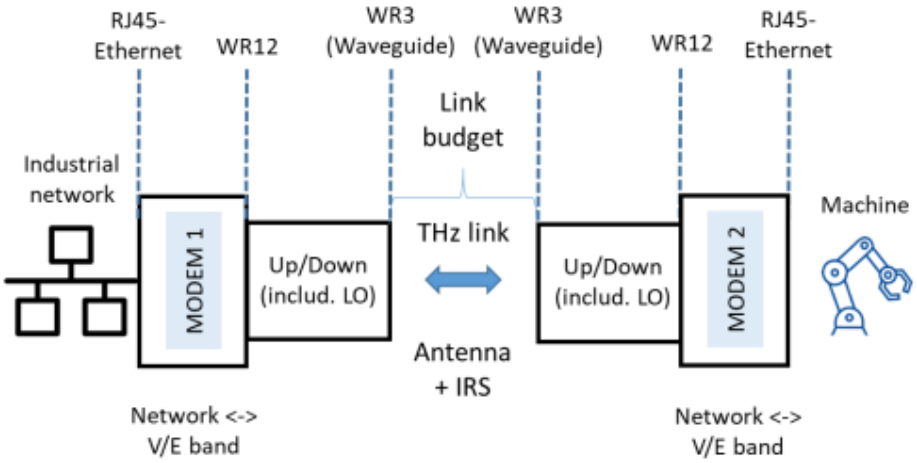

Fig. 1. Network architecture for PoC 1.

The frequencies used in the system are specified in Fig. 2. On the transmit (Tx) side, the FDD modem generates two signals in the E-band: a low channel at 74.7 GHz (L) and a high channel at 84.7 GHz (H). The front-end modules then perform frequency up-conversion to the WR3 band using a phase-locked loop (PLL) that generates a LO signal with an optimum frequency of 25.2 GHz. As a result, radio frequency (RF) signals are produced at 276.3 GHz (L) and 286.3 GHz (H). At the receive (Rx) side, the process is reversed. The incoming RF signal is down-converted using the same LO generation scheme to obtain an E-band signal that can be processed by the FDD modem.

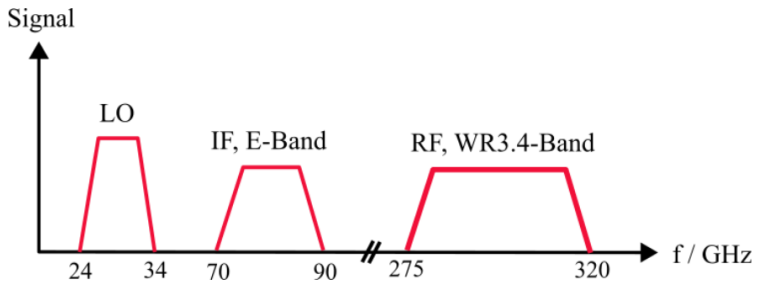

Fig. 2. Frequency bands of LO, IF and RF. Over the Air (OTA) tests are done in WR3.4 band.

2.1.2 OTA link budget

In D6.3, a section was dedicated to estimate the link budget. Within the framework of PoC 1, the scenario is presented in Fig. 3. The actual installation took place at AETNA's Techlab.

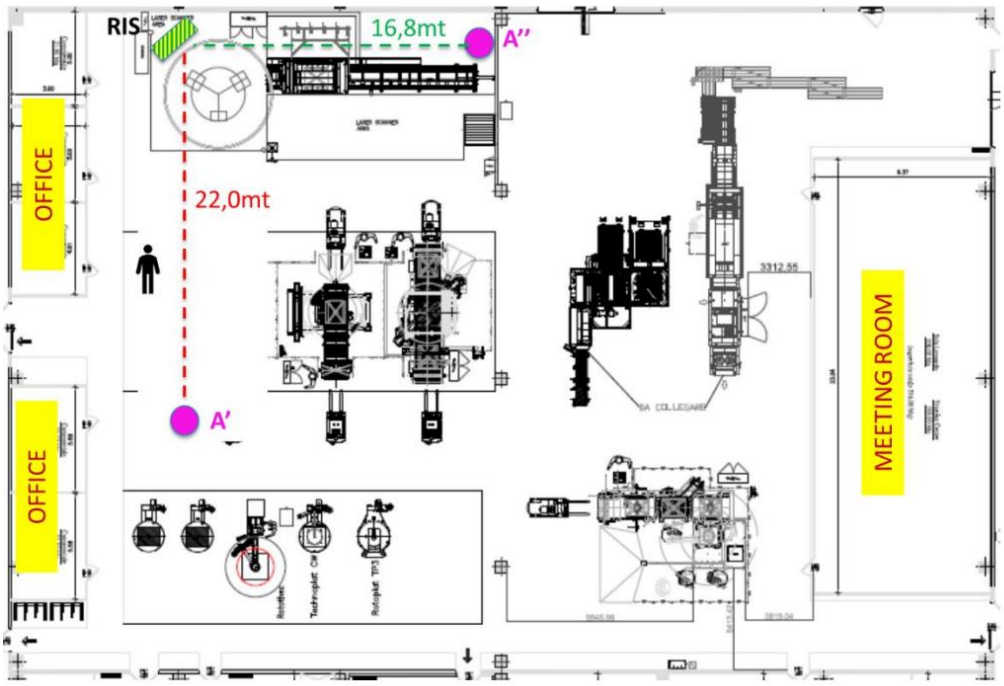

Fig. 3. PoC 1 scenario at AETNA/TECHLAB.

The THz Non-Line of Sight (NLoS) link is established between points A' and A" in the diagram shown, and the distance between these two points is 38.8 m. Thus, the link budget at the two important RF frequencies, considering the second prototype RIS, is

$$L_{\mathrm{Tx-Rx}}(f = 276.3\ \mathrm{GHz}) = 13.2\ \mathrm{dB}$$

$$L_{\mathrm{Tx-Rx}}(f = 286.3\ \mathrm{GHz}) = 12.8\ \mathrm{dB}$$

With the B2B measurements presented in D6.3, we were able to obtain the performances shown in Tab. 1.

Tab. 1. Overview of measured performances.

		WR12 Margin	WR3 Margin	Data-Rate	OTA Link budget	Penalty WR12 -> WR3	OTA Margin
		dB	dB	Gbps	dB	dB	dB
QPSK	FDD	58.1	35	2.55	13.2	23.1	21.8
QAM-16	FDD	47.3	23.6	4.97	13.2	23.7	10.4
QAM-32	FDD	41.6	17	6.23	13.2	24.6	3.8

Thus, we see that in principle, there is sufficient margin for Quadrature Phase Shift Keying (QPSK) and Quadrature Amplitude Modulation (QAM) with 16 states, QAM-16. However, while in QAM-32, a connection will be difficult if there is not excellent alignment of the THz beams.

This table shows that the demonstration of PoC 1 is possible thanks to the work of the project partners on the front-end modules, the diplexers, the high-gain antennas, and the RIS.

2.2 PoC1 at CNRS

This section presents the first over-the-air demonstration of PoC 1, conducted at the IEMN laboratory (CNRS) over a propagation distance of approximately 12 m. This intermediate experiment served as a critical validation step before the full-scale deployment at AETNA, enabling the team to verify system integration, alignment procedures, and link performance under controlled laboratory conditions.

2.2.1 B2B measurements

Prior to the Over-The-Air demonstration, jitter measurements were performed in B2B to determine the network latency as a function of losses induced by a variable attenuator used to simulate free-space propagation. The network infrastructure used for PoC 1 is illustrated in Fig. 4. Four Personal Computers (PCs) are connected in pairs to two switches, which in turn are connected to the Power over Ethernet (PoE) power supplies of the FDD modems. To enable communication between all devices, the four PCs and the two modems are configured within the same subnet. The modems support both 1 Gbps and 10 Gbps links. Although the B2B measurements reported in Deliverable D6.3 were performed using 10 Gbps SFP connections, the demonstration at AETNA-Techlab is conducted using 1 Gbps links. As shown in the figure, PCs 3 and 4 are connected to the switches via 1 Gbps RJ45 cables, while PCs 1 and 2 remain connected to the modems through 10 Gbps SFP links. Communication between the PCs is established using *iperf*, which enables the measurement of data-rate and jitter. Tests are therefore performed between PCs 1 and 2, and between PCs 3 and 4 with:

- Channel 1: PC1 -> PC2
- Channel 2: PC2 -> PC1
- IP link 1: PC3 -> PC4
- IP link 2: PC4 -> PC3

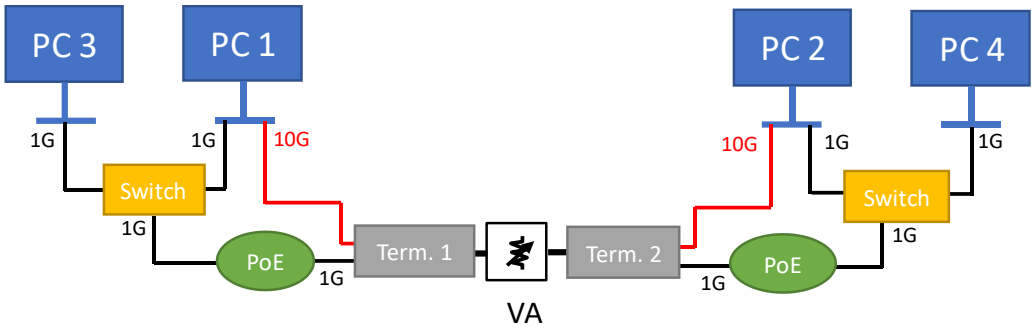

Fig. 4. B2B measurements with network connections. Terminals 1 and 2 are for "Modem + Indoor Unit (IDU) module + high-gain Antenna".

The values obtained for different attenuation values in the case of QPSK modulation are given in the Tab. 2.

Tab. 2. Overview of measured B2B performances for QPSK modulation. The attenuation for which we have the OTA link budget is highlighted in orange (cf. Tab. 1).

QPSK	Ch1				Ch2				IP link 1		IP link 2	
	1G		10G		1G		10G		1G		1G	
Atten (dB)	DR (Gbps)	Jitter (ms)	DR (Gbps)	Jitter (ms)	DR (Gbps)	Jitter (ms)	DR (Gbps)	Jitter (ms)	DR (Gbps)	Jitter (ms)	DR (Gbps)	Jitter (ms)
-35	0.919	0	2.49	0.006	0.928	0	2.49	0.003	0.938	0.017	0.938	0.017
-20	0.918	0	2.49	0.002	0.926	0	2.49	0.03	0.938	0.019	0.937	0.018
-13	0.923	0	2.51	0.011	0.93	0	2.5	0.009	0.937	0.017	0.937	0.019
-10	0.907	0	2.48	0.023	0.918	0	2.5	0.013	0.937	0.019	0.937	0.019

These measurements were also performed for a QAM-16 modulation, and the Tab. 3 is obtained in this case.

Tab. 3. Overview of measured B2B performances for QAM-16 modulation. The attenuation for which we have the OTA link budget is highlighted in orange (cf. Tab. 1).

QAM-16	Ch1				Ch2				IP link 1		IP link 2	
	1G		10G		1G		10G		1G		1G	
Atten (dB)	DR (Gbps)	Jitter (ms)	DR (Gbps)	Jitter (ms)	DR (Gbps)	Jitter (ms)	DR (Gbps)	Jitter (ms)	DR (Gbps)	Jitter (ms)	DR (Gbps)	Jitter (ms)
-24	0.907	0	4.04	0.024	0.918	0	4.02	0.025	0.938	0.023	0.937	0.018
-17	0.923	0	4.05	0.005	0.928	0	4.04	0.019	0.938	0.027	0.937	0.017
-13	0.918	0	4.05	0.007	0.919	0	4.03	0.028	0.937	0.024	0.937	0.019
-10	0.917	0	4.03	0.034	0.926	0	4.05	0.028	0.937	0.027	0.938	0.018

Comparing these two tables, it can be observed that jitter is primarily driven by signal quality rather than modulation order. In the QAM-16 case (Tab. 3), the 10 Gbps link on Ch1 shows a jitter of 0.024 ms at an attenuation of −24 dB, which reduces to 0.005 ms at −17 dB — confirming that a stronger received signal yields more stable latency. Across both tables, the corresponding QPSK values at the same attenuation levels remain in a similar range, suggesting that the choice of modulation has little influence on jitter, and that link margin is the dominant factor.

2.2.2 The RIS panel

For PoC 1, the second passive RIS prototype is not used directly. Instead, an assembly of nine passive RIS units—nominally equivalent to the second prototype—is arranged in a 3×3 panel. However, unlike the single passive RIS prototype, whose optimum frequency in the non-specular configuration is around 282 GHz, the optimum frequency of the RIS panel in the same configuration is closer to 286 GHz. Conversely, at 276 GHz, a drop of approximately 10 dB was observed during characterization measurements using a vector network analyzer (VNA). This asymmetry required additional effort when aligning the Tx and Rx sides, since establishing a link at 286.3 GHz does not necessarily guarantee the same performance at 276.3 GHz. Therefore, the alignment had to be optimized for both frequencies, and the previously computed link budget required further refinement. Nevertheless, a THz link remained achievable for QPSK modulation. In contrast, establishing a link with QAM-16 modulation was more challenging than initially expected, except in cases of near-perfect alignment.

2.2.3 Experimental testbed

2.2.3.1 List of components used

For this demonstration, a number of components were used and are listed below.

- 4× PCs
- 2× Switches
- 2× IDU Modules + Power Supply
- 2× Modems + RJ45 (1 Gbps) and SFP (10 Gbps) network cables + PoE power supply
- 2× Laser pointers
- 1× RIS panel
- 1× Reference metal plate
- 2× High-gain antennas
- 4× Flexible waveguides
- 2× Variable attenuators
- WR12, WR3.4, twists and straight waveguides

2.2.3.2 Setup installation

For OTA measurements, in comparison with Fig. 4, both parts are split and the variable attenuator is removed. The setup installed for the two frequencies is shown in Fig. 5 (a) and (b). The modem + IDU module + antenna terminal assembly was mounted on a breadboard for easier transport to AETNA for the final demonstration. The terminal was then placed on a tripod that could be adjusted along three axes for alignment. Each terminal was paired with a cart containing the two PCs, the switch, and the IDU module's power supply.

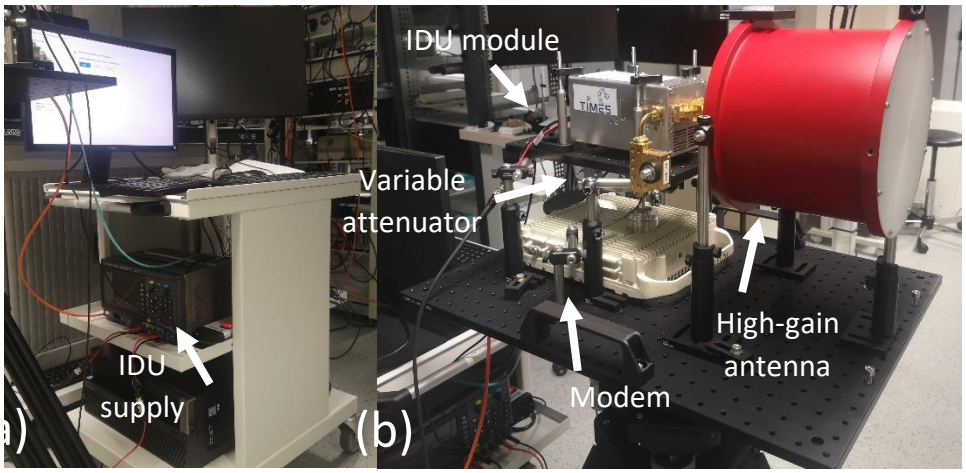

Fig. 5. Photograph of the testbed for one side with (a) PCs and power supply for IDU module and (b) Terminal with the modem, the IDU module and the high-gain antenna.

Since this part of the testbed has already been described previously, we refer the reader to deliverable D6.3 for a more complete description. The high-gain antenna, itself, was connected to the IDU module via a WR3.4 twist to achieve the correct polarization relative to that required for proper operation of the RIS panel. Indeed, the isophase lines of the RIS panel are vertically oriented, so the incident electric field must also be vertical to properly exploit the RIS panel's effect. It should be noted that both high-gain antennas were connected via a twist because the RIS panel does not reverse polarization after reflection.

Regarding the orientation of the RIS panel, we relied on Fig. 6, which shows the different angles for correctly orienting the panel. Thus, whether it was the demonstration at the CNRS or the demonstration at AETNA, the chosen specular configuration was (AoA = 30°, AoD = 30°) and the chosen non-specular configuration was (AoA = 30°, AoD = 60°). This well corresponds to the property of the second prototype RIS, which has an optimum for an AoA – AoD = -30° (Floquet order n = -1, cf. D6.3).

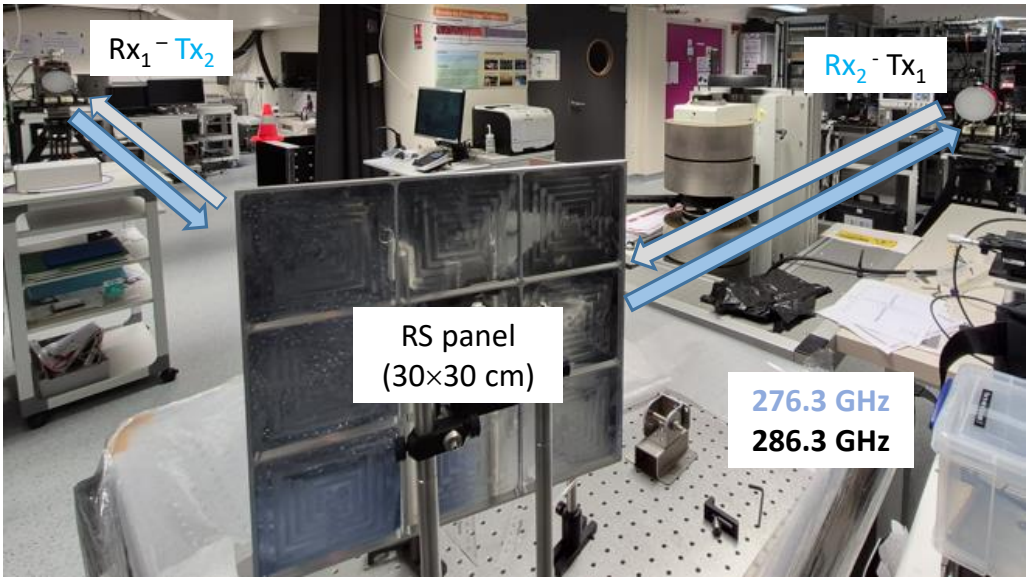

Fig. 6. Photograph of the OTA demo at CNRS showing the 2 terminals.

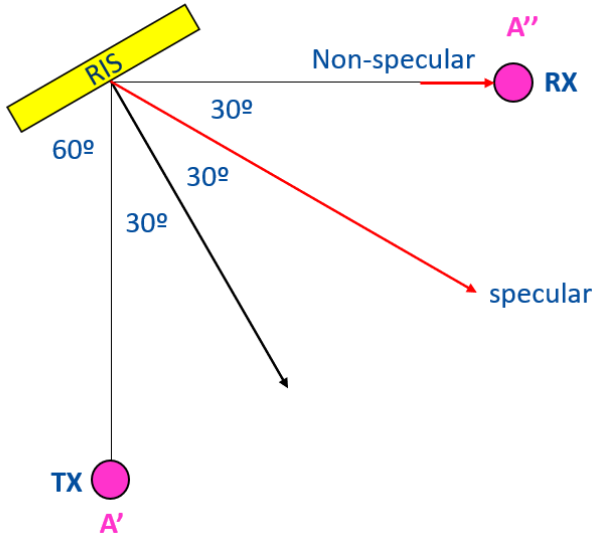

Fig.7. Schematic of the RIS panel orientation for optimum specular and non-specular reflections.

2.2.3.3 Alignment

For alignment, tripods were used to optimize the orientation of the high-gain antennas, and laser pointers were used to visualize the beam positions on the RIS panel, as these are invisible to the naked eye. The RIS panel's own orientation mechanism (cf. Fig. 8) was also used to fine-tune the THz link establishment once a Link Up was achieved on the modems' web interfaces. Proper alignment took some time, but once the link was established, we were able to optimize it effectively using the available tools.

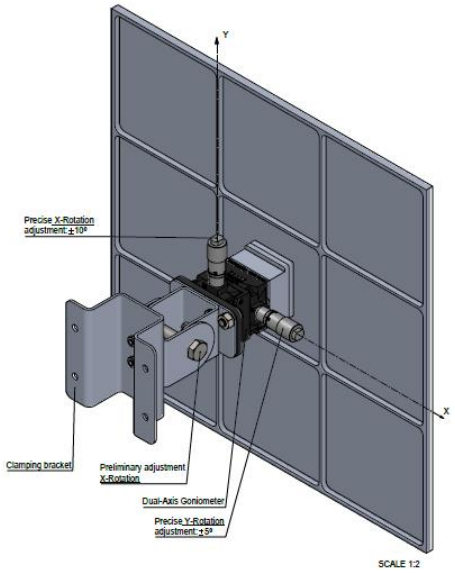

Fig. 8. Schematic of the RIS panel orientation mechanism.

2.2.3.4 Over-the-air performances

The link was established only using QPSK modulation. The modems' web interface provided received signal strength indicator (RSSI) and carrier to interference and noise ratio (CINR) values, while data rate and jitter were obtained via *iperf*. These values are summarized in Tab. 4 and Tab. 5 below.

Tab. 4. Overview of measured OTA performances for QPSK modulation with a Link Up at CNRS.

QPSK	RSSI	CINR	Data-Rate (DR)
	dBm	dB	Gbps
Ch1	-48	17	2.56
Ch2	-47	15	2.59

Tab. 5. Overview of measured OTA performances for QPSK modulation at CNRS.

PC3 -> PC4		PC4 -> PC3	
1G		1G	
DR (Gbps)	Jitter (ms)	DR (Gbps)	Jitter (ms)
0.951	0.02	0.936	0.055

Note: the DR and jitter were measured for 1 Gbps link, that was corresponding to the PoC1 requirements.

Even though the RSSI and CINR values are quite low in QPSK modulation, despite the distance between the terminals being only about 12 m, it is important to note that we are in the very close range of the high-gain antennas, so the received signal is not what we would expect in a far-field setting. We could therefore expect a better RSSI at 39 m, as planned during the final demonstration of PoC 1 at AETNA, which we will now describe.

2.3 PoC1 at AETNA (Final PoC)

Having already detailed the description of the PoC 1 demonstration conducted at CNRS, we will not dwell as much on the same demonstration at AETNA. The most important point to note is that this time, the distance between the two terminals is approximately 39 meters

2.3.1 Setup installation

Platforms shown in Fig. 9 (a) were used to position the terminals, while a tripod was used for the RIS panel as shown in Fig. 9 (b). Platforms are controlled via a console connected to an electrical cabinet.

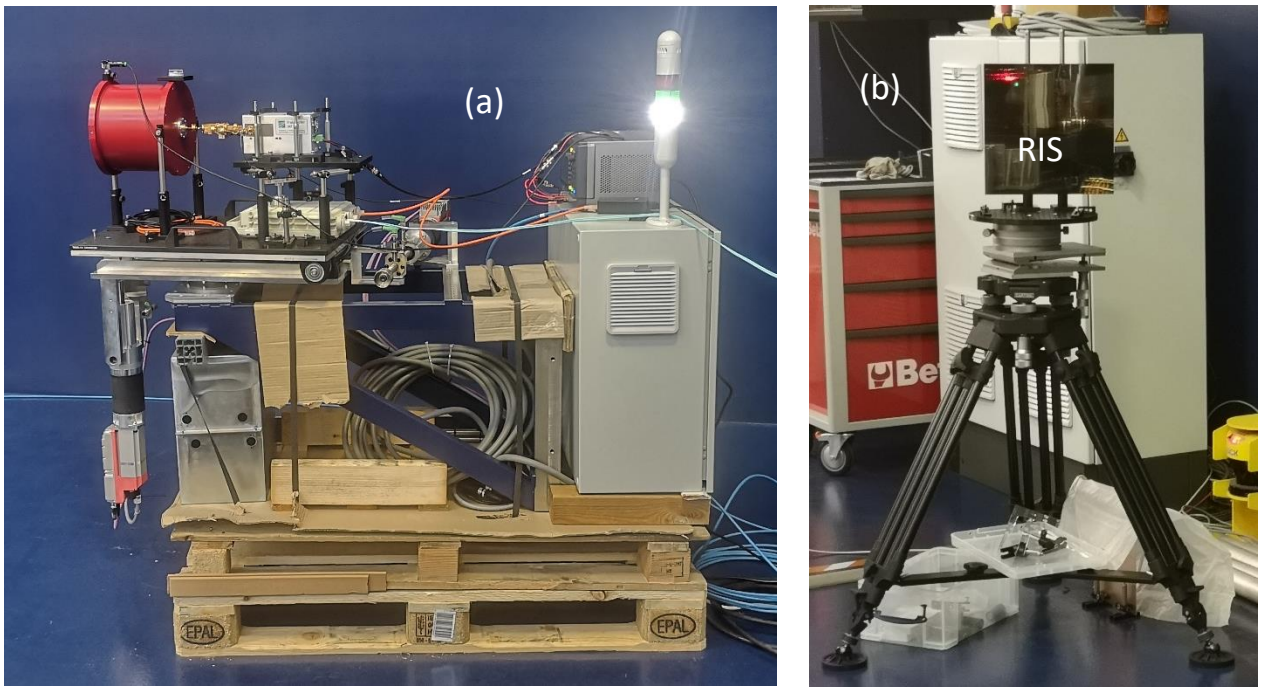

Fig. 9. Photograph of (a) the terminal placed on the plateau from AETNA Company and (b) the RIS panel on a tripod.

The complete electrical installation is shown schematically in Fig. 10 and was developed for this purpose by the company AETNA.

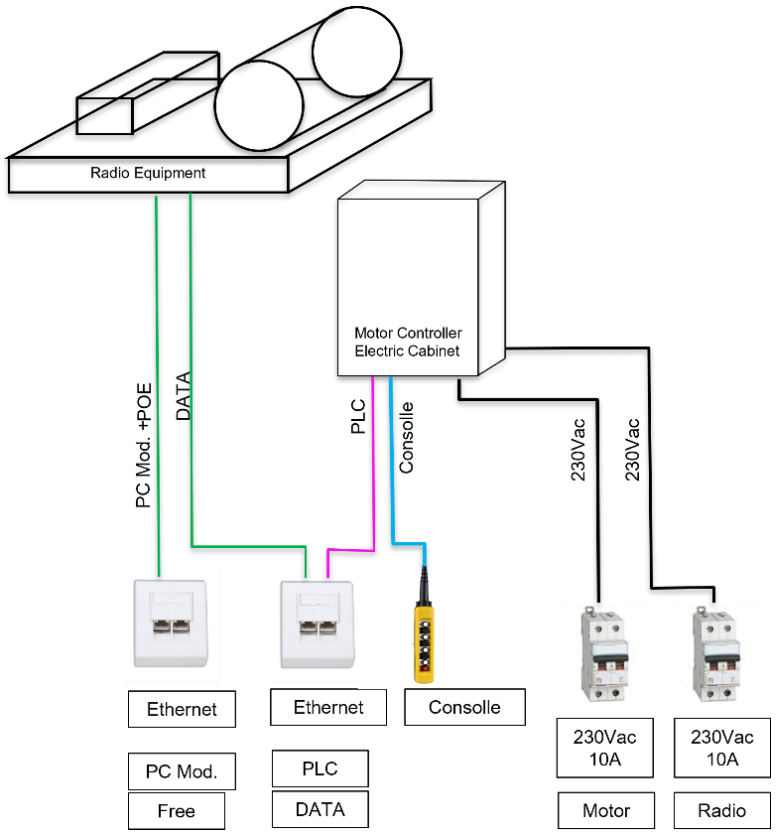

Fig. 10. Schematic of the electrical installation used in the context of PoC 1 at AETNA.

For the PoC 1 demonstration at CNRS, standard PCs were used as PCs 3 and 4, but for the PoC 1 demonstration at AETNA, PCs 3 and 4 were replaced by a Mini PC and an Edge Computer server (cf. Fig. 11) to transfer 10 GB data files each. Otherwise, the rest of the experimental setup remained the same as it was shown in Fig. 5.

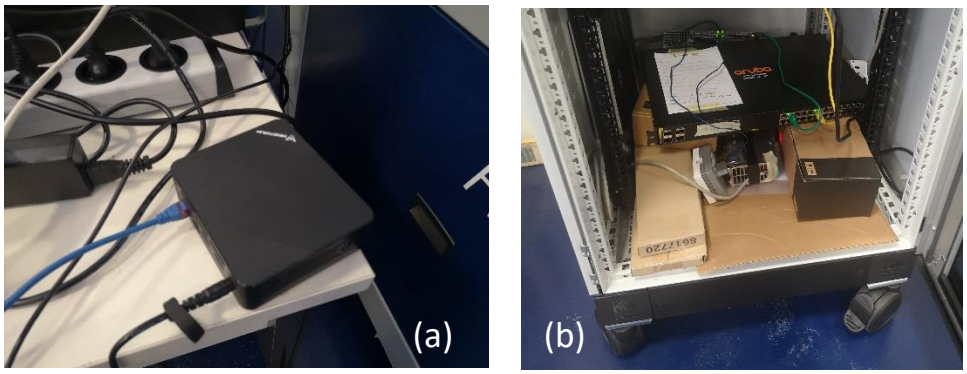

Fig. 11. Photograph of (a) the Mini PC and (b) the EDGE Computer used to transfer 10 GB data files through passive RIS.

Because of the additional losses due to the longer distance, several dB differences were expected in RSSI. Thus, the amplifiers from Fraunhofer IAF partner, which were not used on the laboratory PoC, were placed between the IDU and the diplexer on each terminal to increase a little bit the RSSI even though it would decrease the CINR. At 276 GHz, the additional gain is about 8 dB whereas at 286 GHz, it is closer to 6 dB.

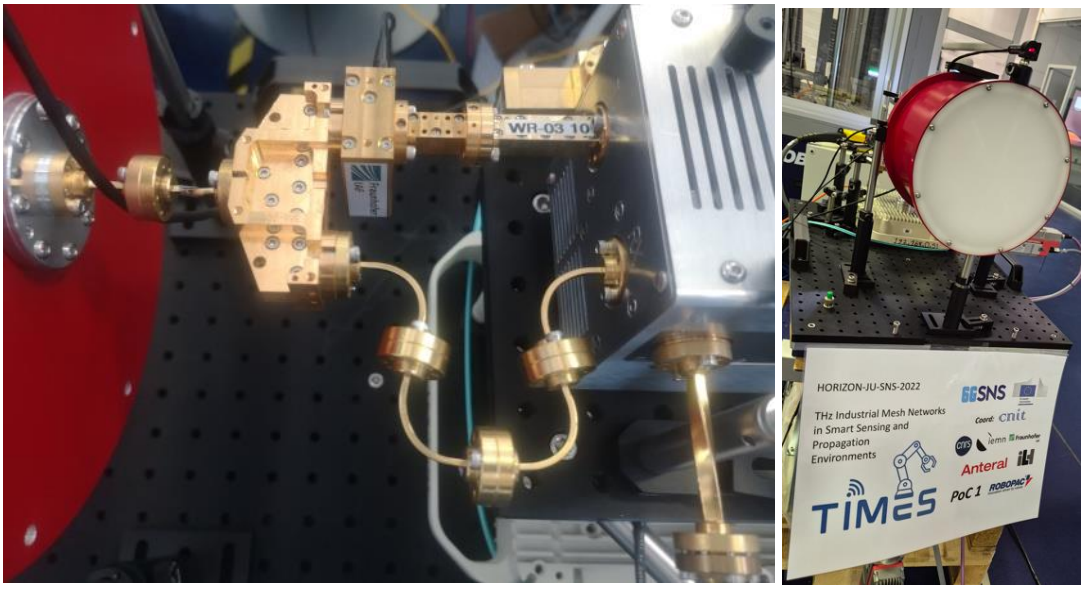

Fig. 12. Photograph of the medium power amplifier (MPA) integrated in the terminal (left) and Terminal 1 (right).

2.3.2 Over-The-Air performance

As we did with the CNRS demonstration, a preliminary alignment was first performed by placing the metallic plate and then the RIS panel in the correct specular and then optimum non-specular configuration. Laser pointers, used to determine the position of the signal emitted by the high-gain antennas and their orientations, were then refined using platforms provided by AETNA, which allowed for more precise angle control. By optimizing step by step the signal between platforms and RIS orientations, this fine tuning

alignment enabled to obtain a link-up for the modems despite the distance, with performance levels noted in Tab. 6.

Tab. 6. Overview of measured OTA performances for QPSK modulation with a Link Up at AETNA.

QPSK	RSSI	CINR	Data-Rate (DR)
	dBm	dB	Gbps
Ch1	-45	18	2.56
Ch2	-43	18	2.56

Since we succeeded in obtaining an 18 dB CINR on both channels despite the MPA added noise, we were able to test a QAM-16 modulation. Indeed, as shown in the D6.3, the minimum CINR to have a QAM-16 is 17 dB. However, the observed DR for QAM-16 was below the expected one, possibly attributed to non-linear effects in the MPA.

Tab. 7. Overview of measured OTA performances for QAM-16 modulation with a Link Up at AETNA.

QAM-16	RSSI	CINR	Data-Rate (DR)
	dBm	dB	Gbps
Ch1	-47	18	4.15
Ch2	-44	18	4.15

Characterization using *iperf* also allowed us to measure the data rate and jitter. These values are reported in Tab. 8 (QPSK) and Tab. 9 (QAM-16).

Tab. 8. Overview of measured OTA KPIs for QPSK modulation at AETNA.

Ch1				Ch2				PC3 -> PC4		PC4 -> PC3	
1G		10G		1G		10G		1G		1G	
DR (Gbps)	Jitter (ms)	DR (Gbps)	Jitter (ms)	DR (Gbps)	Jitter (ms)	DR (Gbps)	Jitter (ms)	DR (Gbps)	Jitter (ms)	DR (Gbps)	Jitter (ms)
0.919	0	2.59	0.015	0.93	0	2.56	0.009	0.944	0.02	0.936	0.046

Tab. 9. Overview of measured OTA KPIs for QAM-16 modulation at AETNA.

Ch1				Ch2				PC3 -> PC4		PC4 -> PC3	
1G		10G		1G		10G		1G		1G	
DR (Gbps)	Jitter (ms)	DR (Gbps)	Jitter (ms)	DR (Gbps)	Jitter (ms)	DR (Gbps)	Jitter (ms)	DR (Gbps)	Jitter (ms)	DR (Gbps)	Jitter (ms)
0.92	0	4.15	0.06	0.93	0	4.15	0.006	0.944	0.02	0.936	0.046

From these tables, it can be observed that the RSSI values at AETNA are only approximately 3 dB lower than those recorded during the laboratory PoC at CNRS, despite the significantly longer propagation distance. It should be recalled that power amplifiers are now integrated in the chain, which partially compensates for the additional free-space path loss. It is also worth noting that the near-field beam quality at the antenna output, as well as the beam quality following reflection off the RIS panel, cannot be precisely characterised. Nevertheless, the relatively modest RSSI reduction suggests that operating at 39 m places the antennas in a more established far-field regime.

Tab. 10. Overview of measured OTA KPIs for the PoC1 and comparison with estimated values at the beginning of the project.

	Estimated	**PoC1**
DR (NLoS)	5 Gbps	4.1 Gbps
Reliability	10-3	< 10-3
Latency	128µs	< 500 µs
Jitter	2 µs	9-16 µs

2.4 Conclusions of the PoC1

To conclude, we successfully established a 300 GHz THz free-space link using a passive RIS. The system was first demonstrated at the IEMN laboratory (CNRS, France) over a distance of approximately 12 meters, and subsequently at AETNA Robopac (Italy) over about 40 meters. At AETNA, leveraging an MPA from Fraunhofer, we achieved 16-QAM modulation with a data rate of 4.15 Gbps, a jitter of 0.006 ms, and an error rate of approximately 5.4%.

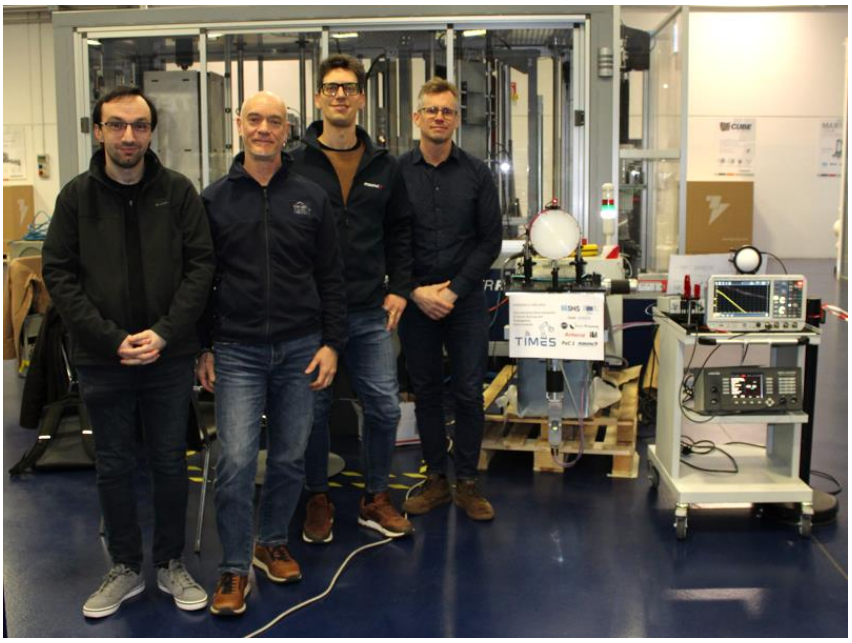

Fig. 13. Photograph PoC1 team: F. Dutin (CNRS), G. Canini (Robopac), C. Lanzoni (Robopac), Prof. G. Ducournau (CNRS).

3 PoC-2: Dynamic THz Link with Beam-Steering by Leaky-Wave Antenna

3.1 Technical Update

This section presents the updates achieved for PoC-2 since the publication of Deliverable D6.3 [5]. In [5], the focus was on the integration of the hardware components and the initial validation of the THz communication link and beam-steering concepts. The present deliverable reports the progress obtained during the subsequent experimental campaigns and provides updated results based on the improved measurement setups and extended testing activities.

PoC-2 investigates dynamic THz communication scenarios in which the direction of the radiated beam can be controlled to maintain connectivity under changing geometrical conditions. Two complementary approaches are considered within this PoC. The first approach is based on frequency-dependent beam steering using a leaky-wave antenna (LWA), where the radiation angle is determined by the operating frequency. The second approach investigates the use of a reconfigurable intelligent surface (RIS) to enable non-line-of-sight (NLoS) communication by redirecting the THz signal toward the receiver.

Both approaches are evaluated through dedicated experimental campaigns that extend the work presented in D6.3. The following subsections summarize the updates obtained for the LWA-based beam-steering link and for the RIS-assisted link, respectively, highlighting the progress achieved since the previous deliverable.

3.1.1 System Overview of the LWA Beam-Steering Setup

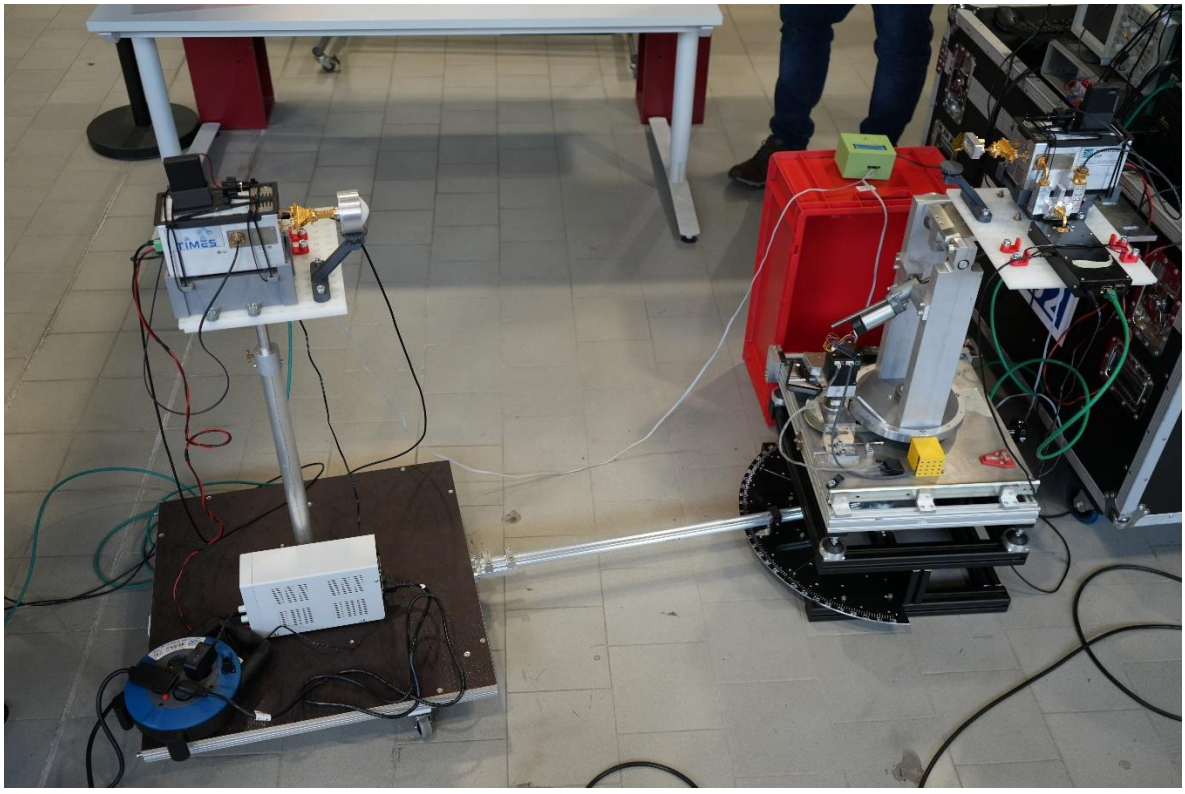

Fig. 14: Experimental setup of the LWA beam-steering measurements using the Kurvenmeister system.

The experimental setup used for the LWA-based beam-steering measurements is shown in Fig. 14 and follows the system architecture previously introduced in [5]. The setup consists of the TIMES modem, the THz Indoor Units (IDUs), and the RF front-ends operating in the 300-GHz band. The base station (BS) integrates the LWA, whose radiation angle depends on the operating frequency. By tuning the operating frequency, the main beam direction can be adjusted without mechanical steering, enabling the THz link to maintain connectivity under changing geometrical conditions. On the mobile station (MS), a lens horn antenna (LHA) is used.

Compared to the configuration described in [5], the measurement setup has been further refined to allow systematic characterization of the frequency-dependent beam steering behavior. The BS is mounted in a fixed position. The MS is mounted on a mechanical positioning structure that constrains the receiver to move along a circular trajectory around the transmitter while maintaining a constant propagation distance. This mechanical structure, referred to as the *Kurvenmeister*, uses a rigid arm to keep the receiver at a fixed distance of 1 m from the transmitter while the relative angle between BS and MS can be varied in a controlled manner.

Another important update compared to the earlier laboratory setup is that the measurement system has been relocated to an industrial-like environment. This allows the performance of the dynamic THz link to be evaluated under conditions that are closer to realistic industrial deployment scenarios, while still maintaining controlled geometrical conditions for repeatable measurements.

3.1.2 System Overview of the RIS-Assisted THz Link Setup

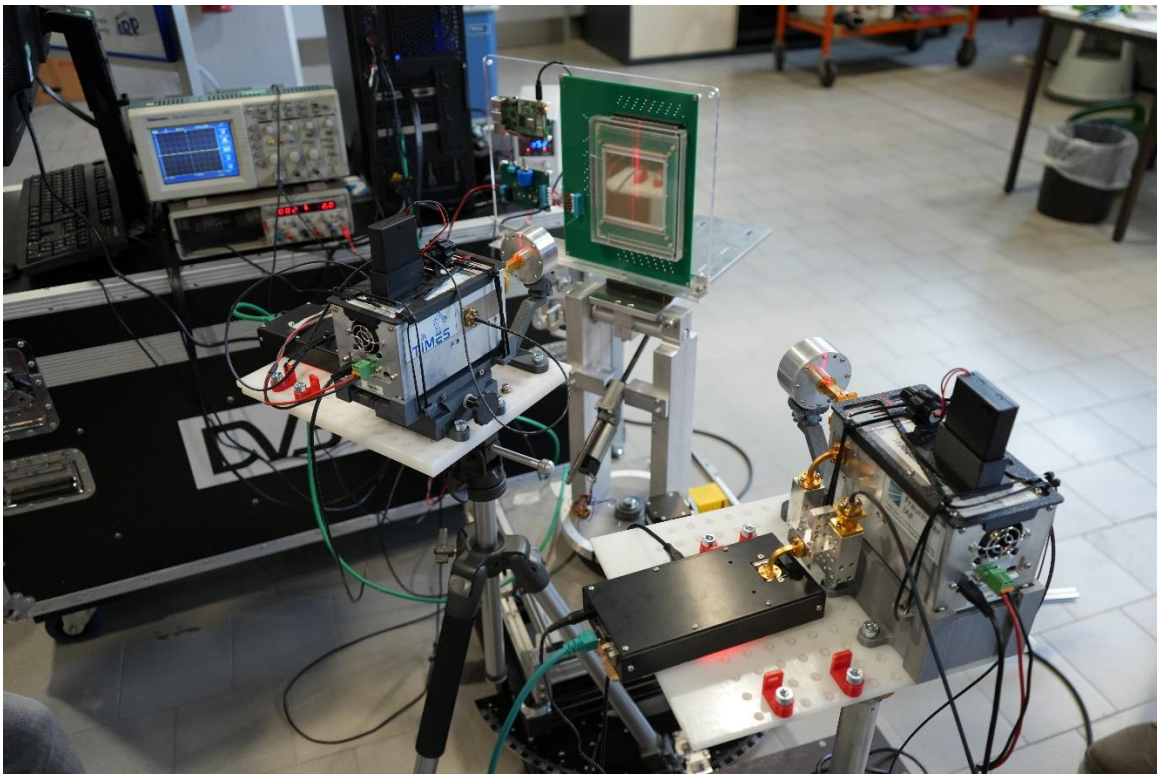

Fig. 15: Experimental setup of the RIS-assisted measurements.

The experimental setup used for the RIS-assisted measurements is shown in Fig. 15 and follows the general system architecture introduced in [5]. As in the LWA-based setup, the system consists of TDD modems, the THz IDUs, and the RF front-ends operating in the 300 GHz band.

The RIS is placed between BS and MS and is used to redirect the signal toward the receiving side in a NLoS configuration. Both BS and MS are equipped with LHAs that illuminate the RIS and receive the reflected signal. The RIS itself is mounted on a dedicated mechanical holder that allows precise alignment of the surface relative to both stations.

Compared to the configuration described in [5], the experimental setup has been adapted to investigate RIS-assisted links under controlled short-range conditions. The BS and MS units are mounted on separate tripods, allowing flexible positioning and accurate alignment of the antennas. This configuration makes it possible to place the antennas as close as possible to the RIS to minimize the propagation distance and compensate for the high path losses at THz frequencies.

This setup enables controlled evaluation of both specular and non-specular reflection scenarios while maintaining precise alignment of the RIS, BS, and MS within the measurement environment.

3.1.3 Experimental results of the LWA-based Setup

Following the integration phase reported in [5], additional experimental measurements were carried out to further characterize the performance of the LWA-based beam-steering link. The focus of these measurements was to experimentally verify the frequency-dependent steering behaviour of the leaky-wave antenna and to quantify the achievable data rate as a function of both the operating frequency and the relative angle between the BS and the MS.

In addition to the mechanical improvements, a dedicated frequency control interface was implemented to simplify the adjustment of the operating frequency. The interface allows the operating frequency of all four local oscillators (LOs) to be changed simultaneously using two control buttons. Furthermore, a software routine was implemented that continuously sends link request messages between the modems. This mechanism allows the system to automatically establish or re-establish the link whenever a connection is required, which significantly simplifies the identification of viable link configurations.

Using the improved experimental setup, a measurement campaign was conducted in which the achievable data rate was recorded for different steering angles and operating frequencies. The results are summarized in Fig. 16, which shows a heatmap of the measured data rate as a function of the relative angle between the BS and the MS and the operating frequency of the system. In the figure, white areas indicate configurations where no link could be established, while dark blue regions correspond to configurations where a link could be detected but no data transmission was achieved. The remaining coloured regions represent successful data transmission, with the colour scale indicating the measured data rate.

The results clearly demonstrate the frequency-dependent beam-steering behaviour of the leaky-wave antenna. For each operating frequency, the highest data rates are observed within a limited angular range corresponding to the main radiation lobe of the antenna. As the operating frequency changes, this region shifts along the angular axis, confirming that the beam direction can be controlled through frequency tuning. This behaviour enables the THz communication link to follow the relative movement between BS and MS without requiring mechanical steering of the antenna. Based on this principle, a continuous link without connection loss during simultaneous position and frequency change was demonstrated, as described in section 3.2.

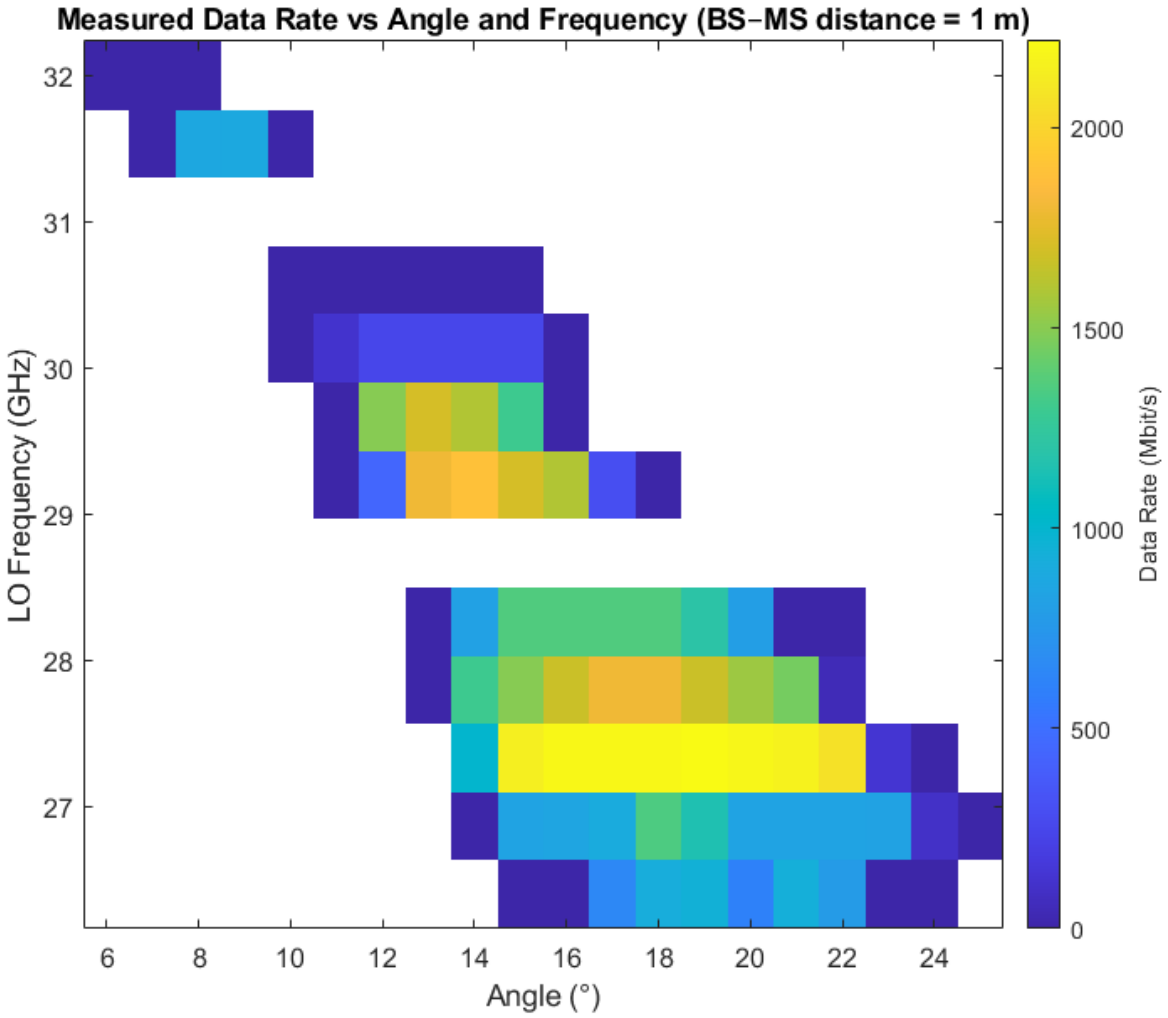

Fig. 16: Measured data rate as a function of beam angle and operating frequency for the LWA-based THz link at a BS-MS distance of 1 m. White areas indicate configurations where no link was established.

Experimental results of the RIS-assisted setup

In an initial measurement campaign, the RIS was investigated with the assumption that the reflection angle could be controlled by the applied voltage. For this purpose, configurations with angle of arrival (AoA) of 0° and angle of departure (AoD) values between ±15° and ±30° were tested over an LO frequency range from 26.0 to 30.4 GHz, corresponding to RF frequencies from 268.48 to 303.68 GHz. Both horizontal and vertical polarizations were considered, while the applied voltage was varied between 1 V and 12 V. The distances were set to 1.2 m between BS and RIS and 1 m between RIS and MS. No communication link could be established in any of the tested configurations. In addition, channel sounder measurements showed a scattered component, but this behaviour was not dependent on the applied voltage. These results indicate that no voltage-dependent beam steering could be demonstrated with this setup.

Based on the results of the initial measurements and the information provided in [3], the operating principle of the RIS was reinterpreted. It was assumed that the non-specular reflection is only activated at sufficiently high bias voltage. Furthermore, changing the applied voltage does not modify the steering angle of the reflected beam. Instead, for a fixed AoA, the resulting AoD depends only on the operating frequency, while

the applied voltage primarily affects the reflection amplitude. Under these assumptions, the RIS can be interpreted as an on-off device, where the applied voltage controls whether the non-specular reflection mechanism is active.

Before further RIS measurements were conducted, the performance limits of the communication system were evaluated using OTA LoS measurements without the RIS. For this purpose, two LHAs with a gain of 35dBi each were used at an operating frequency of 278.08 GHz. In a first setup, a stable communication link with a data rate of 2.2 Gbit/s was achieved over a distance of 18 m. The distance could not be further increased due to space limitations in the robotic laboratory.

In a second setup, a 20-dB attenuator was inserted into the RF path to emulate higher path losses and determine the practical link threshold of the system. At 3.9 m, a data rate of 1.5 Gbit/s was achieved, corresponding to a calculated path loss of approximately 43.15 dB. When the distance was increased to 4.5 m, a link could still be established but no data transmission was possible, resulting in a calculated path loss of approximately 44.5 dB. This value therefore represents the practical link threshold of the system. The calculated path losses include all components located after the RF combiner, including the additional 20 dB attenuator.

To normalize the RIS measurements with respect to the results reported in [3], the properties of the specular reflection of the RIS were first investigated. For this purpose, a measurement was conducted with equal angles of arrival and departure (AoA = AoD = 30°), corresponding to a specular reflection scenario. The distance between the BS and the RIS was set to 1.53 m, while the distance between the MS and the RIS was 1.25 m, resulting in a total propagation distance of 2.78 m. The measurements were performed at an operating frequency of 278.08 GHz with a 20-dB attenuator included in the RF path, which was also considered in the path loss calculation.

Under these conditions, a data rate of approximately 200 Mbit/s was achieved, indicating that the link was already close to collapse. Increasing the distance further resulted in a complete link failure. From the measured configuration, a total link loss of 40.52 dB was calculated for the entire path. By comparing this value with the previously determined practical link threshold of approximately 44.5 dB, the additional loss introduced by the specular RIS reflection can be estimated to be approximately 4 dB.

Based on the measured specular RIS loss, a link budget estimation for the non-specular RIS case was derived. According to the results reported in [3], the RIS exhibits an approximate loss of 22 dB for specular reflection and about 45 dB for non-specular reflection, resulting in an additional loss of roughly 23 dB for the non-specular case. Combining this value with the measured specular RIS loss of approximately 4 dB in our setup leads to an estimated additional non-specular loss of about 27 dB.

Using this estimate, the achievable propagation distance for the non-specular RIS configuration was approximated. Based on the previous analysis, the additional loss introduced by the RIS in the non-specular case was estimated to be approximately 27 dB. Since the measurement setup allowed frequency tuning only in steps of 3.2 GHz, an additional margin of about 3 dB was considered to account for possible frequency mismatch between the optimal RIS operating frequency and the available modem frequencies. This results in an expected total additional loss of approximately 30 dB for the non-specular RIS reflection.

To compensate for part of this additional loss in the experimental setup, the previously inserted 20dB attenuator was removed. Compared to the specular measurement configuration, the remaining difference therefore corresponds to approximately 10 dB additional loss. Assuming free-space path loss scaling, a 10 dB

increase in path loss corresponds to a reduction of the achievable propagation distance by approximately a factor of 3.2. Based on the previously measured specular path length of 2.78 m, the expected distance for a non-specular RIS link was therefore estimated to be approximately 0.87 m.

It should be noted that these link budget calculations assume far-field propagation conditions. Since the distances used in the experiments approach the near-field region, small variations in the propagation distance can lead to significant deviations from the calculated link budget, potentially resulting in both better and worse link performance than predicted under far-field assumptions.

Based on the previously derived link budget estimation, a dedicated experimental setup for the non-specular RIS case was implemented. The distances between the BS and the RIS were adjusted to 27–28 cm, while the distance between the RIS and the MS was set to 46–47 cm, resulting in a total propagation distance of approximately 0.73–0.75 m. The distance could not be further reduced due to mechanical limitations of the setup. A frequency sweep over all available modem frequencies was performed, and the angles ±30° and ±50° were tested, which were identified as the most promising configurations according to [3].

The measurements showed that for angles of ±30° and +50°, no modem response was observed at any frequency. For an angle of −50°, reproducible timeouts were detected, indicating that a link attempt was recognized by the modem, but only at an LO frequency of 27.6 GHz. Once the link was externally established, it could be maintained, but no data transmission was possible. Furthermore, switching the RIS off resulted in an immediate link collapse, confirming that the observed behaviour was directly related to the RIS. The effect was only observed when the RIS was operated at maximum bias voltage, which is consistent with the previously assumed on/off behaviour of the device.

These observations indicate that the link budget in the tested configuration was very close to the required threshold. Consequently, it was concluded that only a few additional dB of link margin would likely be sufficient to enable a stable non-specular RIS-assisted link with successful data transmission.

To obtain the additional link margin required for successful data transmission, the RF path was further optimized. In the original setup, a fixed 10 dB attenuator was placed between the WR-12 splitter and the IDU. This component was replaced by a variable attenuator, allowing the attenuation in this part of the signal path to be reduced. The best results were obtained with an attenuation of 0.5 dB.

Using this optimized configuration, stable non-specular RIS-assisted links could finally be established. For an AoD of 50°, the best performance was achieved at an LO frequency of 27.6 GHz, resulting in a data rate of 730 Mbit/s. At the same angle, a data rate of 150 Mbit/s was measured at 27.2 GHz, while only 20 Mbit/s was achieved at 28.0 GHz under otherwise identical conditions. No connection could be established at other frequencies. For an AoD of 30°, the best frequency was again 27.6 GHz, yielding a data rate of 200 Mbit/s, while no connection was observed at other frequencies. Measurements for an AoD of 40° could not be performed due to mechanical limitations of the setup.

Additional observations further confirmed the RIS-assisted nature of the link. All connections were immediately lost when the RIS was switched off, and reducing the applied bias voltage resulted in a corresponding reduction of the achievable data rate.

3.2 Industrial Validation

To validate PoC-2 under realistic industrial constraints, the experimental campaign was structured around two complementary configurations. First, the LWA beam-steering setup demonstrates how a THz link can be

dynamically optimized by tuning frequency to maintain high throughput and sub-millisecond latency across different pointing angles. Second, the RIS-assisted setup investigates how a current/voltage-adjustable reflective surface can enable THz connectivity in NLoS conditions, potentially extending coverage in cluttered industrial layouts where obstacles and occlusions are common.

3.2.1 LWA Beam-Steering Setup

BI-REX reviewed and validated the PoC-2 experimental campaign as an industrially relevant scenario, demonstrating that a **dynamic THz point-to-point link** can sustain **very low latency** and **multi-Gbps throughput** while adapting the radiated beam direction through **frequency-controlled beam steering** of a **LWA**. This behavior is particularly valuable for industrial applications where conventional wireless technologies (e.g., Wi-Fi) may not satisfy the combined constraints of **latency**, **determinism**, and **sustained data rate**, especially in the presence of high-bandwidth sensors and real-time control loops.

Test setup and methodology

The validation test was structured around three operating frequencies, selected to cover a controlled angular range while maximizing link quality and achievable data transfer:

- **26.800 GHz** used for beam angles approximately in the range **24° to 21°**
- **27.200 GHz** used for beam angles approximately in the range **21° to 14.5°**
- **29.200 GHz** used for beam angles approximately in the range **14.5° to 11°**

During the experiment, the operating frequency was adjusted to ensure that the LWA operated close to the optimal steering condition for the target angle, thereby maximizing received signal quality and overall link performance. The performance was monitored through network-level indicators (throughput and latency) and validated with practical measurements (speed test and ping). Additionally, screen recordings of throughput, ping, and the currently selected operating frequency were collected as evidence of the dynamic behavior and to support traceability of the results.

Frequency [GHz]	Range [°]
26.800	**24°-21°**
27.200	**21°-14.5°**
29.200	**14.5°-11°**

Observed performance

The measured results confirm that frequency selection is an effective steering and optimization mechanism for the considered link:

- **Throughput** varied depending on the angular position and corresponding beam visibility, ranging from approximately **300 Mbps** at the edge conditions (i.e., near the borders of the usable signal region) up to about **2.3 Gbps** in the best visibility region, observed approximately between **21° and 15°**.
- **Latency (ping)** remained consistently **below 1 ms** across stable frequency conditions, confirming suitability for low-latency industrial communication.
- During **frequency transitions**, latency temporarily increased for a short interval (typically **a few seconds**), then returned to the nominal sub-millisecond level once the new frequency setting

stabilized. This effect is consistent with the transient reconfiguration time required for frequency switching and link re-stabilization.

Overall, the test confirms a clear operating region in which the THz link provides both high throughput (multi-Gbps) and low latency, while still maintaining usable connectivity in less favorable steering conditions.

Industrial relevance and validation by BI-REX

BI-REX considers this scenario **high-value for industrial deployments** in which wireless communication must support either:

1. **Deterministic/low-latency control traffic**, where sub-millisecond performance is beneficial (e.g., control interfaces close to PLC-grade requirements, real-time monitoring/control), and/or
2. **High-throughput sensor streaming**, where multi-Gbps capacity can enable advanced perception and inspection workflows (e.g., **3D LiDAR**, **real-time 3D video scanning**, or high-resolution multi-camera acquisition for quality control and digital twin updates).

In these contexts, Wi-Fi connectivity can be limited by variable contention, unpredictable latency, and throughput fluctuations, especially in harsh RF environments or congested industrial sites. The proposed LWA-based THz link, instead, offers a strong candidate approach for **short-range, high-capacity, low-latency wireless backhaul** in factory and logistics environments, provided that line-of-sight (or controlled propagation conditions) can be maintained.

Proposed deployment concept on mobile robotics (MiR 250)

BI-REX also assessed a concrete and realistic industrial exploitation path by considering the **MiR 250 mobile robot** as a target platform for PoC integration. This platform is particularly compatible with the PoC requirements for two reasons:

- The MiR 250 provides **accurate localization and pose information**, and its position can be accessed via **available APIs**. This information can be used to predict the relative angle between transmitter and receiver and thus determine the optimal LWA operating frequency.
- The frequency can be **dynamically controlled** using an **out-of-band control channel** (e.g. Wi-Fi) to select the frequency that maximizes beam alignment, ensuring that the LWA operates in its best steering/visibility region during robot motion.

From an industrial standpoint, this enables practical architecture where the THz link is used as a **high-throughput payload channel** (e.g., for sensor data), while a separate conventional channel provides **control-plane coordination** for frequency/beam optimization. The MiR platform is also expandable with advanced payloads such as **4K / high-resolution 3D cameras**, whose real-time streaming can quickly exceed the capability of standard wireless technologies. In such cases, PoC-2 can provide the missing wireless "backbone" needed to support real-time remote perception and edge/cloud processing.

Future enhancements and scalability

As a future evolution, BI-REX identified a potential improvement aimed at increasing autonomy and reducing dependency on out-of-band localization/control. The concept is to enhance the LWA transmitter architecture to support **two frequencies simultaneously**, enabling a dual-function operation:

- **Frequency A** maintains the active high-quality data link ("anchor" frequency).
- **Frequency B** periodically scans alternative frequencies in time slots to assess whether a better steering condition is available.

Based on measured link quality metrics, the system could then perform an **automatic frequency hand-off** to the best candidate frequency, minimizing disruption and reducing or eliminating the need for an external control channel and/or external localization systems. This approach would improve robustness for mobile scenarios and would be aligned with industrial expectations for self-optimizing connectivity under dynamic conditions.

Validation conclusion

Based on the observed throughput/latency performance, the stable sub-millisecond latency, and the ability to optimize the link through frequency-driven beam steering, BI-REX validates PoC-2 as a **promising solution for industrial wireless connectivity** in scenarios that require **high data rate**, **low latency**, and **controlled directional communication**, with a clear pathway for integration on mobile robotic platforms and a credible roadmap toward more autonomous operation.

3.2.2 RIS-Assisted THz Link Setup

BI-REX considers RIS-assisted THz links as **potentially relevant** for industrial environments characterized by occlusions and highly "topological" layouts (e.g., dense shopfloors, corridors, racks, machinery), where maintaining strict LoS is often impractical and where mobile robots may temporarily operate in **shadowed areas**. In this context, a current/voltage-adjustable reflective surface can become a **connectivity enabler**, redirecting THz energy around obstacles and extending coverage to otherwise **unreachable** zones.

From the current experimental evidence, the setup is **functional but still limited** in terms of robustness and achievable data rates across configurations. For the tested conditions, best results were obtained at **27.6 GHz** (LO/fundamental setting) with around **730 Mbit/s** at **AoD 50°** (0.5 dB attenuation), while other nearby frequencies showed a strong degradation (e.g., 150 Mbit/s at 27.2 GHz; 20 Mbit/s at 28.0 GHz under the same setting). At **AoD 30°**, the best observed performance was around **200 Mbit/s** at **27.6 GHz**, and no link was achieved at other tested frequencies; **AoD 40°** could not be measured due to mechanical constraints. Moreover, turning the RIS off causes the link to drop, and decreasing the applied voltage reduces the achievable data rate, confirming the RIS bias as a key lever (and sensitivity) for link operation.

While the present performance and sensitivity make this approach **less immediately deployable** than the LWA beam-steering case, RIS-assisted THz remains strategically interesting as a **coverage-extension tool** for NLoS pockets in factories—especially for mobile robotics, where recurring occlusions can be mitigated by placing one (or more) reconfigurable reflective surfaces in critical locations to "bend" connectivity into shadowed work areas.

AoD [°]	Best Performance [Mbit]	Frequency [GHz]
50	730	27.6
40	200	27.6
30	N/A	N/A

Additional activities

It is worth mentioning that during the project we explored the possibility to industrially exploit Terahertz frequencies for sensing, not only for communication, in particular evaluating THz technologies for non-contact moisture sensing in ceramic materials. For reference, a parallel comparison was conducted against solid-state radar technology operating in a similar sensing configuration. The results show that both approaches can be integrated into automated industrial systems for real-time monitoring. THz sensing operates in the **0.1–3 THz frequency range**, where electromagnetic waves strongly interact with water molecules, making it highly sensitive to moisture: the system measures **signal attenuation and propagation delay**, which increase with water content due to strong absorption of THz radiation. This makes THz especially effective for **high-resolution, surface or near-surface moisture detection**, although its penetration depth is limited in wetter materials. Overall, while radar offers robustness and deeper penetration, THz frequencies provide superior intrinsic sensitivity for moisture sensing applications, enabling precise characterization of material properties in industrial quality control contexts.

4 References

[1] TIMES deliverable (D2.3) "Definition of the scenarios and KPI for hardware demonstration and PoC", Available on TIMES Website, http://www.times6g.eu/deliverables.

[2] TIMES deliverable (D5.3) "Design, fabrication and verification of high directivity and beam steering antennas at THz frequencies", Available on TIMES Website, http://www.times6g.eu/deliverables.

[3] Times deliverable (D5.4) "Development and validation of IRS-based THz links", Available on TIMES Website, http://www.times6g.eu/deliverables.

[4] Times deliverable (D6.2) "Integration and validation of MODEM+RF Front ends", Available on TIMES Website, http://www.times6g.eu/deliverables.

[5] TIMES deliverable (D6.3) "Full integration of the 300 GHz PoC", Available on TIMES Website, http://www.times6g.eu/deliverables.

Grand Agreement No: 101096307

Full Title: THz Industrial Mesh Networks in Smart Sensing and Propagation Environments

Start date: 01/01/2023

End date: 31/12/2025

Duration: 36 Months

Appendix to D6.4

Electromagnetic Field (EMF) Exposure at THz Frequencies

Document Type	
Title	Appendix to D6.4 - Electromagnetic Field (EMF) Exposure at THz Frequencies
Contractual due date	31/03/2026
Actual submission date	17/03/2026
Nature	Report
Dissemination Level	PUB
Lead Beneficiary	TNOR, TUBS
Responsible Author	Per Hj Lehne (TNOR), Varvara Elesina (TUBS)
Contributions from	Per Hj Lehne (TNOR), Varvara Elesina (TUBS), Georg Jensen (TUBS)

Revision history

Version	Issue Date	Changes	Contributor(s)
v0.1	29/01/2026	Initial Version, inputs to sections 2 and 3	Per Hj Lehne (TNOR)
v0.2	09/02/2026	Inputs to sections 2	Varvara Elesina (TUBS), Georg Jensen (TUBS)
v0.3	27/02/2026	Inputs to sections 2 and 3	Varvara Elesina (TUBS), Georg Jensen (TUBS)
v0.4	09/03/2026	Inputs to section 4	Varvara Elesina (TUBS)
v0.5	16/03/2026	Introduction, Scope, Structure and Conclusion	Varvara Elesina (TUBS)
v0.6	17/03/2026	Formatting	Varvara Elesina (TUBS)
v1	15/04/2026	Final Version Approved	Luca Sanguinetti (CNIT), Thomas Kurner (TUBS)

Table of Contents

List of Abbreviations

THz Terahertz

RIS Reconfigurable intelligent surface

LoS line-of-sight

MPC multipath component

NLoS non-line-of-sight

Rx receiver

Tx transmitter

ERP equivalent radiated power

EIRP equivalent isotropically radiated power

EMF Electromagnetic field

RF radio frequency

SAR specific absorption rate

RMS root mean square

POI point of investigation

FDTD finite difference time domain

MoM method of moments

Executive Summary

This document reviews the state of knowledge and practical assessment approaches for Electromagnetic field (EMF) exposure at low-THz and THz frequencies, with particular focus on the industrial communication scenarios addressed in the TIMES project. The motivation is that current RF-EMF exposure frameworks and regulations are well established up to 300 GHz, while future low-THz and THz applications increasingly extend toward and beyond this boundary. At the same time, TIMES considers industrial deployments with short distances, large antenna apertures, worker accessibility, dynamic operation, and complex propagation environments, all of which make exposure assessment more challenging than in conventional far-field macro-cell scenarios.

1 Introduction

Radiation safety and the potential health effects of exposure to non-ionizing electromagnetic fields (EMF) have been studied for decades. Public attention to this topic increased significantly with the introduction and widespread use of mobile telephones since the 1980s. The first widely recognized guidelines and recommended safety limits for radio-frequency (RF) exposure were published by the International Commission on Non-Ionizing Radiation Protection (ICNIRP) in 1998 and were later updated in 2020 [1].

These guidelines cover the frequency range from 100 kHz to 300 GHz. With the growing research interest in 6G technologies, attention has increasingly shifted toward even higher frequencies, including the THz range. This development also creates a need to investigate possible EMF exposure and health-related issues beyond 300 GHz.

The Smart Networks and Services Joint Undertaking (SNS JU) has explicitly included EMF-related objectives in its 6G vision and annual work programmes. In particular, for TIMES, responding to the call in the SNS Work Programme 2021–2022 [2], EMF is addressed in several places.

Related to the United Nations Sustainable Development Goals (UN SDGs), the work programme states:

> "In addition, complementary societal issues, such as ethical issues in the context of privacy or Electric and Magnetic Fields (EMF) awareness and reduction, are targets of the SNS WP."

Related to Stream B, the programme further states:

> "This continuum must provide users with improved performance, higher level of control, increased transparency in interactions with digital services, adequate support of ethical values and conformance with societal requirements and readiness (e.g., GDPR, EMF awareness, etc.) whilst contributing to key SDGs."

It also highlights:

> "Increased spectrum efficiency . . . , and also addressing citizen concerns like low EMF exposure."

In relation to Call B-01-02 – Expected outcomes and scope, the programme states:

> "Technologies and architectures enabling support of new higher efficiency mobile communication approaches, such as cell-free networking, with capability to drastically reduce energy consumption and to control EMF exposure levels."

In addition, it notes:

> "Human-friendly radio systems: . . . It also covers antenna systems for EMF control and awareness to minimise human exposure . . . "

Overall, the EMF-related objectives of the SNS JU can be summarized in four main points:

- Safety
- Awareness
- Control
- Reduction

In 2022, the 5G-PPP established a task force that published the white paper "Beyond 5G/6G EMF Considerations" [3], providing proposals and recommendations on EMF-related topics for the SNS JU.

1.1 Scope

This deliverable provides an overview of EMF exposure assessment issues relevant to low-THz and THz wireless systems, with particular emphasis on the industrial deployment scenarios investigated in the TIMES project. It reviews the current regulatory and technical background for exposure assessment up to 300 GHz and discusses the main open questions and practical interpretation challenges for frequencies above 300 GHz.

The document further summarizes established EMF assessment approaches based on relevant ITU recommendations and examines their applicability to THz industrial environments. In this context, it addresses both measurement-based and calculation-based assessment methods, including their practical limitations, with special attention to near-field exposure conditions and the influence of multipath propagation.

The deliverable is intended as a technical basis for understanding how EMF compliance and exposure evaluation may need to be adapted for future THz industrial systems. It does not define new exposure limits and does not provide a complete product- or site-specific compliance procedure for all THz applications. Instead, it aims to identify the most relevant assessment challenges, summarize available methods, and highlight the industrial low-THz scenarios in which further methodological development is most needed.

1.2 Structure

The rest of the document is structured as follows:

- Section 2 presents the overview of the EMF radiation safety levels.
- Section 3 summarizes the assessment methods.
- Section 4 analyses TIMES scenarios.
- Section 5 concludes the report.

2 Survey on THz and radiation safety

EMF exposure limits in the radio frequency (RF) domain are typically specified up to 300 GHz, reflecting the frequency range commonly addressed by major compliance standards and assessment frameworks [4], [5]. This is broadly consistent with the ITU Radio Regulations, where the spectrum above 275 GHz has historically been used mainly under special regulatory conditions, and only a limited part has been considered for active terrestrial applications. However, the spectrum above 275 GHz is not unused: it supports passive services such as radio astronomy and earth/space observation, and it is also addressed by some short-range communications standards. At the same time, driven by growing interest in low-Terahertz (THz) and THz technologies for future wireless systems, regulatory and technical studies are increasingly extending beyond 300 GHz, including work related to potential future allocations.

One example is the THz physical layer defined in IEEE Std 802.15.3d-2017 [6]. This PHY is intended for wireless switched point-to-point applications and operates in a frequency range from 252 GHz to 321 GHz, see the allocation plan in Figure 1 from [7]. It supports channel bandwidths between 2.16 GHz and 69.12 GHz and is designed to achieve nominal physical-layer data rates of up to approximately 100 Gbit s^{-1}.

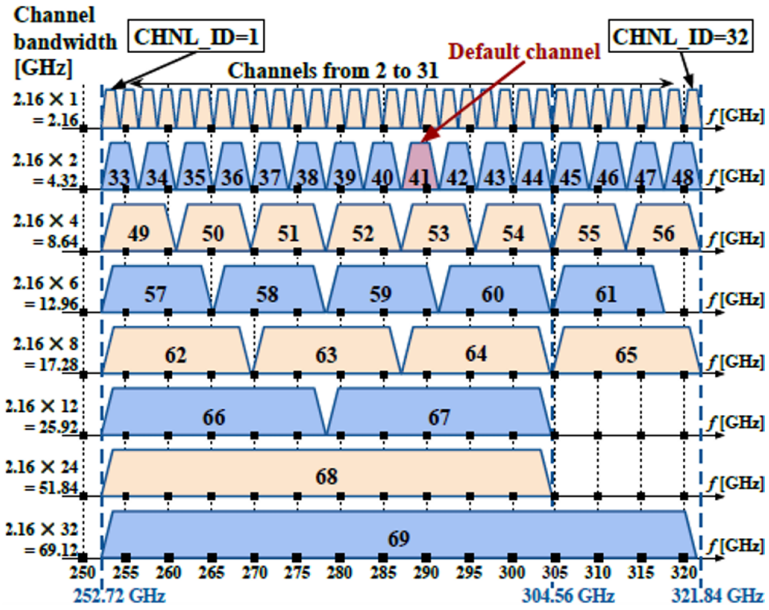

Figure 1: IEEE Std 802.15.3d-2017 bandwidth allocation plan from 252 GHz to 321 GHz [7].

In addition to communication-related applications, electromagnetic fields in the frequency range above 300 GHz are also used in medical applications, particularly within the THz spectral range. THz radiation has been applied for in vivo imaging of human skin [8], where a quantum cascade laser tuned to 2.85 THz was used to detect skin lesions and potential skin cancers. Similarly, malignant breast cancer tissue has been identified in freshly excised breast tissue samples using a THz pulsed spectrometer operating in the frequency range of 0.15 THz to 2.0 THz [9]. Furthermore, freshly excised brain tissue has been imaged with a reflection-type THz time-domain imaging system operating at approximately 0.3 THz to 1.3 THz [10].

Beyond biomedical diagnostics, THz radiation is also used for non-destructive evaluation and security screening. In these applications, THz waves can penetrate many non-conductive materials such as clothing, paper, and plastics, enabling the detection of concealed objects or internal structures without damaging the investigated sample. Various THz imaging systems exploit this property by illuminating objects with radiation in the approximate frequency range of 0.1 THz to 10 THz and detecting the reflected or transmitted signals. In practical implementations, specific frequencies such as 395 GHz and 650 GHz are used, while sensor arrays capture the returning radiation to reconstruct two-dimensional images of the inspected object [11].

Consequently, it is timely to review the current regulatory landscape above 300 GHz and discuss possible implications for human exposure assessment.

This chapter first summarizes the existing exposure and compliance framework up to 300 GHz and then reviews the status of knowledge and open issues for frequencies above 300 GHz, extending toward the THz and infrared range.

2.1 RF exposure limits up to 300 GHz

National regulations generally draw on two major families of exposure limits. In many regions, the limits are based on the ICNIRP guidelines, which cover the frequency range from 100 kHz to 300 GHz [1]. These guidelines are widely referenced in public-health assessments, including by the World Health Organization (WHO). In the United States, exposure limits are set by the Federal Communications Commission (FCC) and are largely derived from ANSI/IEEE Std. C95.1 [12], [13].

In Europe, ICNIRP-based limits are adopted in most countries, although several countries apply more restrictive constraints (e.g., Belgium, Switzerland, Italy, Croatia, Bulgaria, and Greece). The FCC-based limits are also used in other jurisdictions, including Canada, and are applied in part in countries such as Japan and South Korea.

Importantly, adoption and implementation can differ depending on whether the limits target device compliance, typically expressed via specific absorption rate (SAR) for near-body use or environmental/network exposure, typically assessed via incident field levels or power density.

Table 1 summarizes the global adoption of EMF exposure limits for both mobile devices and network infrastructure. It distinguishes between device limits, typically expressed in terms of the SAR, and network limits for antennas, usually based on field strength or power density. The table shows that most countries follow the ICNIRP guidelines, while a smaller number apply the FCC 1996 limits or other national approaches.

Table 1: The global adoption of SAR and network limits for EMF exposure (number of countries) [14]

	ICNIRP 1998 or 2020	FCC 1996	Other
Device limits (SAR)	158	19	37
Network limits (antennas)	137	10	37

ICNIRP-based limits are widely adopted in many countries, supported by their broad international use in public-health assessments and, in the European context, by a largely harmonized regulatory approach.

Exposure limits are fundamentally specified as basic restrictions,which relate to quantities inside the human body that are linked to established adverse health effects—primarily tissue heating and resulting temperature rise. Because these internal quantities are generally not accessible for routine compliance testing, they are complemented by the reference levels, which are expressed in terms of external, measurable quantities in the environment, such as electric field strength, magnetic field strength, or incident power density. In practice, compliance assessments typically compare measured or computed environmental fields against the reference levels, if the reference levels are met under the applicable conditions, compliance with the corresponding basic restrictions is ensured by construction.

2.1.1 Basic restrictions

Basic restrictions are defined in terms of internal dosimetric quantities that are directly related to established adverse effects, i.e., tissue heating. Depending on frequency, the limits are expressed either via SAR (below 6 GHz) or via absorbed power density S_{ab} (above 6 GHz) [5].

Table 2: Basic restrictions for whole-body (averaging interval of 30 min) and local exposure (averaging interval of 6 min). [1], [5]

Exposure scenario	Frequency range	Whole-body average SAR ($W\,kg^{-1}$)	Local Head/Torso SAR ($W\,kg^{-1}$)	Local Limb SAR ($W\,kg^{-1}$)	Local S_{ab} ($W\,m^{-2}$)
Occupational	100 kHz – 6 GHz	0.4	10	20	NA
	>6 GHz – 300 GHz	0.4	NA	NA	100
General public	100 kHz – 6 GHz	0.08	2	4	NA
	>6 GHz – 300 GHz	0.08	NA	NA	20

Specific absorption rate (SAR) for $f \leq 6$ GHz. The SAR quantifies the rate at which electromagnetic energy is absorbed per unit mass of tissue [4], [5]:

$$\mathrm{SAR} \triangleq \frac{\mathrm{d}}{\mathrm{d}t}\left(\frac{\mathrm{d}W}{\mathrm{d}m}\right) \quad [\mathrm{W\,kg^{-1}}], \tag{1}$$

where W is absorbed energy and m is the tissue mass element. In dosimetric modelling, SAR is often evaluated as $\mathrm{SAR} = \sigma|E|^2/\rho$, with tissue conductivity σ, rms electric field strength in tissue E, and tissue mass density ρ [4]. To reflect thermal time constants, SAR limits use defined averaging: whole-body average SAR is averaged over 30 min, while local SAR is averaged over 6 min and over any contiguous 10 g of tissue [5].

Absorbed power density S_{ab} for $f > 6$ GHz. At THz frequencies, absorption occurs predominantly in superficial tissue layers. Therefore, the basic restriction is expressed as absorbed power density S_{ab} [$\mathrm{W\,m^{-2}}$], i.e., the power absorbed per unit area at the body surface [5]. For compliance purposes, S_{ab} is time-averaged over 6 min and spatially averaged over 4 $\mathrm{cm^2}$. For $f > 30$ GHz, an additional constraint is applied for small exposure spots: the absorbed power density averaged over 1 $\mathrm{cm^2}$ shall not exceed twice the corresponding 4 $\mathrm{cm^2}$ restriction [5].

2.1.2 Reference levels

From the basic restrictions discussed above, ICNIRP [1] has derived reference levels for the electromagnetic field exposure values which could result in the whole body or local temperature rise as described above. Table 3 contains the reference levels for whole-body average, and Table 4 contains the reference levels for local exposure above 400 MHz as defined by ICNIRP.

For frequencies from 400 MHz to 6 GHz, the reference levels are evaluated as peak spatial values over the projected whole-body area. For frequencies from 6 GHz to 300 GHz, the incident power density is spatially averaged over a projected body surface area of 4 $\mathrm{cm^2}$. For frequencies above 30 GHz, an additional constraint applies where the exposure averaged over 1 $\mathrm{cm^2}$ must not exceed twice the limit specified for 4 $\mathrm{cm^2}$.

Table 3: ICNIRP (2020) reference levels above 400 MHz, averaged over the whole body and 30 min [1] [15]

Exposure scenario	Frequency range	Incident E-field strength; E_{inc} ($\mathrm{V\,m^{-1}}$)	Incident H-field strength; H_{inc} ($\mathrm{A\,m^{-1}}$)	Incident power density; S_{inc} ($\mathrm{W\,m^{-2}}$)
Occupational	400 MHz to 2000 MHz	$3\sqrt{f_M}$	$0.008\sqrt{f_M}$	$f_M/40$
	2 GHz to 300 GHz	NA	NA	50
General public	400 MHz to 2000 MHz	$1.375\sqrt{f_M}$	$0.0037\sqrt{f_M}$	$f_M/200$
	2 GHz to 300 GHz	NA	NA	10

The values for power density are summarized in Figure 2 below.

Table 4: ICNIRP (2020) reference levels for local exposure above 400 MHz, averaged over 6 min [1] [15]

Exposure scenario	Frequency range	Incident E-field strength; E_{inc} (V m^{-1})	Incident H-field strength; H_{inc} (A m^{-1})	Incident power density; S_{inc} (W m^{-2})
Occupational	400 MHz to 2000 MHz	$3\sqrt{f_M}$	$0.008\sqrt{f_M}$	$0.29\, f_M^{0.86}$
	2 GHz to 6 GHz	NA	NA	200
	6 GHz to 300 GHz	NA	NA	$275/f_G^{0.177}$
	300 GHz	NA	NA	100
General public	400 MHz to 2000 MHz	$1.375\sqrt{f_M}$	$0.0037\sqrt{f_M}$	$0.058\, f_M^{0.86}$
	2 GHz to 6 GHz	NA	NA	40
	6 GHz to 300 GHz	NA	NA	$55/f_G^{0.177}$
	300 GHz	NA	NA	20

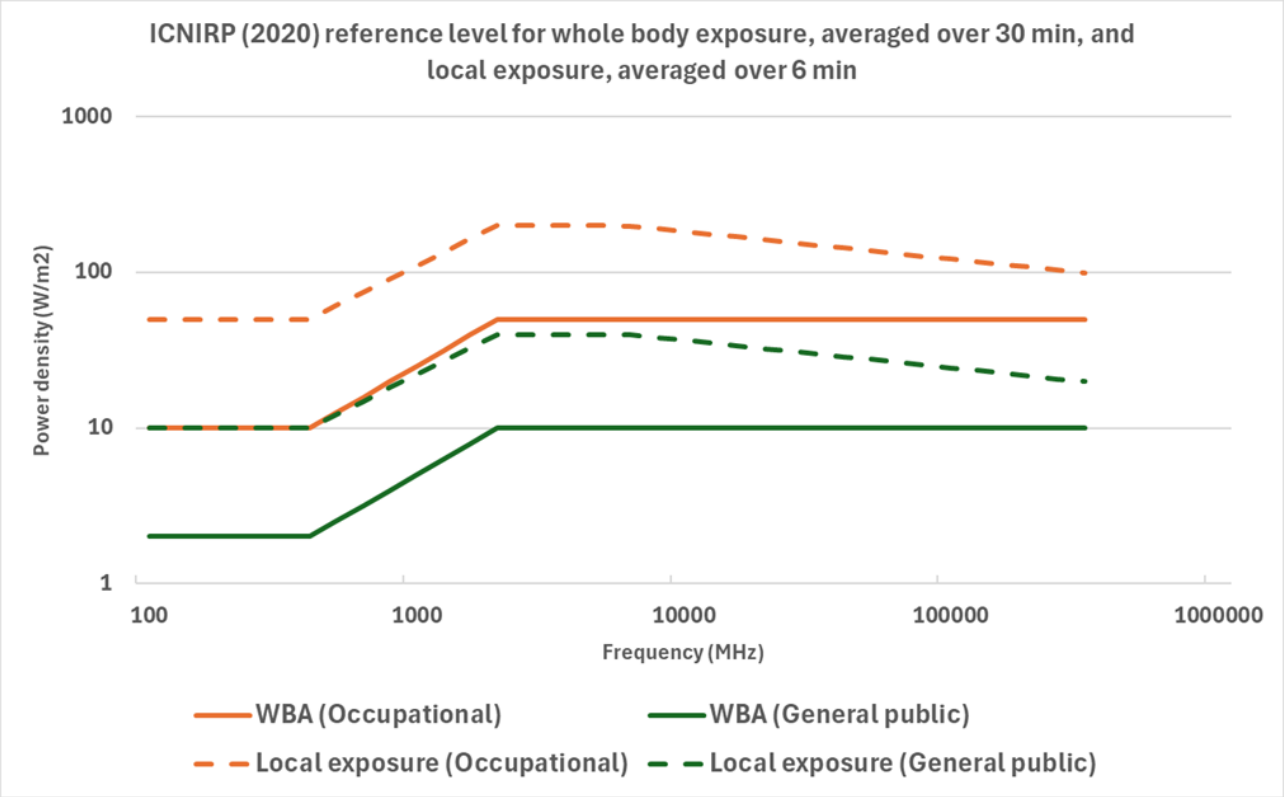

Figure 2: ICNIRP (2020) reference levels for occupational and general public, whole-body average over 30 minutes and local exposure over 6 minutes. [1]

2.2 Exposure beyond 300 GHz

EMF exposure limits and reference levels are not defined for frequencies above 300 GHz by ICNIRP, nor any other body. There are however studies on the effects of radiation exposure for higher frequencies.

In the radiation safety context, frequencies above 300 GHz are discussed in the context of infrared (IR). The sub-THz and THz ranges overlap with with far infrared radiation (FIR). Two different classifications of IR are currently used. The International Commission of Illumination (CIE) has classified IR radiation according to the International Lighting Vocabulary (ILV) . The International Standards Organization (ISO) specifies a different classification (ISO 20473 [16]). These are summarized in Table 5 and Figure 3.

Table 5: Infrared radiation classifications.

	CIE	ISO 20473
Near infrared	IR-A: 0.7 µm to 1.4 µm (215 THz to 400 THz)	NIR: 0.78 µm to 3.0 µm (100 THz to 384 THz)
Mid infrared	IR-B: 1.4 µm to 3.0 µm (100 THz to 215 THz)	MIR: 3.0 µm to 50 µm (6 THz to 100 THz)
Far infrared	IR-C: 3.0 µm to 1000 µm (0.3 THz to 100 THz)	FIR: 50 µm to 1000 µm (0.3 THz to 6 THz)

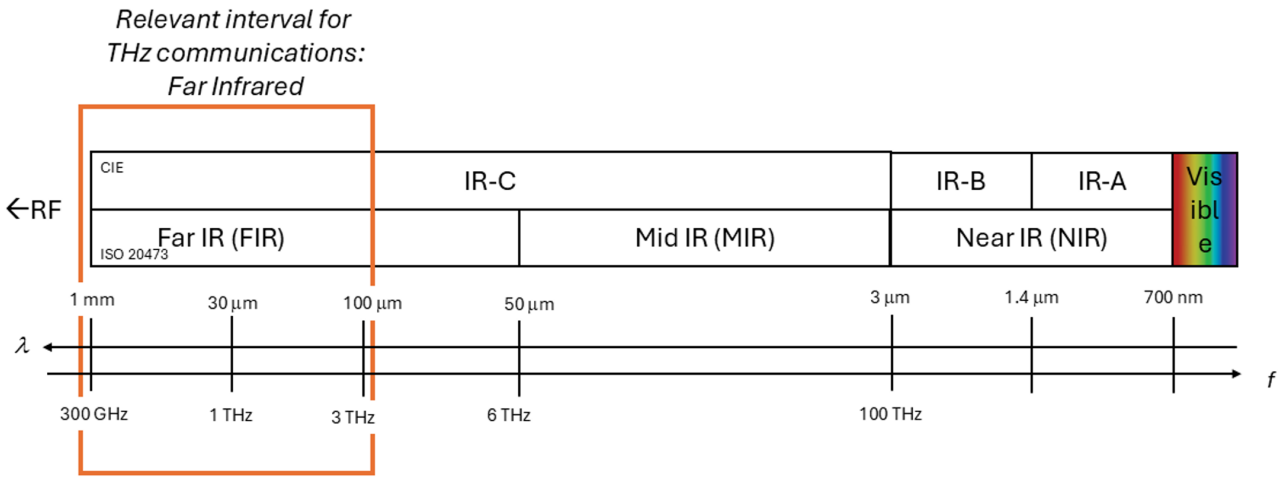

Figure 3: Definitions of the infrared wavelengths and relevant wavelengths considered for THz communications.

ITU spectrum regulations extend beyond 300 GHz up to 3 THz. Up to 1 THz, frequency identifications[1] exist, mostly for passive services. The range from 1 THz to 3 THz is also regulated, but currently, no frequency identification exists. The relevant frequency range then overlaps with the far infrared band, as shown in Figure 3.

2.2.1 Safety regulations for frequencies beyond 300 GHz

Since this frequency range above 300 GHz is also defined as infrared radiation, safety regulations also exist for this. This is also covered by ICNIRP in two specific guidelines published in 2013, one covering incoherent visible and infrared radiation [17], and one covering laser radiation [18]. Both cover the wavelength span up to 1 mm, which corresponds to a frequency of 300 GHz.

Scope and relevance In general, both guidelines assist the development of principles of protection against optical, including laser radiation hazards. They are *"intended for use by the various experts and national and international bodies who are responsible for developing regulations, recommendations, or codes of practice to protect workers and the general public from the potentially adverse effects of optical radiation."* In contrast to the ICNIRP guidelines for electromagnetic fields up to 300 GHz (wavelengths greater than 1 mm) these guidelines do not differentiate between occupational and public exposure.

The optical radiation guidelines focus mainly on the wavelengths shorter than 3 µm (IR-A and IR-B). For incoherent radiation. far infrared (IR-C) is considered less of a problem, assuming that non-laser sources are not emitting enough power above 3 µm to cause health hazards other than the possibility of heat stress. Neither incoherent nor laser guidelines target communication technology scenarios. Laser usage for communications

[1] Identification is a definition of a frequency band for a specific use in accordance with a resolution from the ITU-R World Radiocomnication Conference (WRC). This does not preclude the use of the frequency band by any other ITU-R service to which they are identified and does not establish priority for a specific ITU-R service.

is currently confined to space communications, namely intersatellite links in LEO systems like Starlink, Kuiper, OneWeb, etc. There is some interest also in space-to-ground applications. In any case, these applications are not likely to impose a hazard for humans due to the natural separation distance being a characteristic of the scenarios. Therefore, the following discussion will not include laser technologies.

Optical radiation exposure is typically measured as irradiance and radiant exposure. Irradiance, EIR, is the imposed power density ($\mathrm{W\,m^{-2}}$) on a surface, while radiant exposure, HIR represents the dose ($\mathrm{J\,m^{-2}}$). This means that it should be possible to compare the Irradiance limit value for IR with the local exposure levels for RF up to 300 GHz (see Table 4).

The ICNIRP guidelines on incoherent visible and infrared radiation does not provide particular limit values for IR-C above 3 µm wavelength. Currently known sources of contribution to the spectral region 3 mm to 1000 mm are arc and incandescent sources and the statement is that this is normally of no practical concern from a health hazard standpoint. [17] [19]. However, it is also stated that the partial irradiance that is in this spectral range can contribute to the actual physical exposure.

Recommended limit values for the irradiance in the wavelength range 780 nm to 3000 nm (IR-A and IR-B) is given by the equations [17]:

$$E_{IR}^{BL} = \begin{cases} 18\,t^{-0.75} \cdot 10^{3}\,\mathrm{W\,m^{-2}}, & t < 1000\,\mathrm{s} \\ 100\,\mathrm{W\,m^{-2}}, & t > 1000\,\mathrm{s} \end{cases} \tag{2}$$

The exposure time, t, is the main parameter in the equation. This added exposure for spectral wavelengths above 3 µm is accounted for by setting the exposure limit to a corresponding level. This is explained with an example in [17]:

"For instance, for a thermal radiator with a surface temperature of 1000 °C, about 50 % of the total irradiance is contained in the wavelength range above 3000 nm, so that ***when the part below 3000 nm is limited to 100 W m^{-2}, the permitted total irradiance equals about 200 W m^{-2}****. This is well below levels that have induced cataract in an industrial setting."*

Consequently, the nearest we come to an exposure limit for IR-C is an irradiance of $200\,\mathrm{W\,m^{-2}}$.

2.2.2 Guideline consistency below and above 300 GHz

In Section 2.1.2, Table 3 and Table 4, the RF-EMF exposure limits at 300 GHz (1 mm wavelength) is defined. In the previous section, we found that the nearest interpretation of an exposure limit for IR-C is $100\,\mathrm{W\,m^{-2}}$ for exposure times longer than 1000 s (16.7 min), where no distinction is given between public and occupational exposure. The discussion on IR-C sources indicates that the exposure scenarios, however, are typical occupational. A summary of the values is given in Table 6.

Table 6: Summary of exposure limits below and above 300 GHz

	RF-EMF @ $f = 300$ GHz		IR-C @ $\lambda < 1$ mm
	Whole body exposure	Local exposure	
Average time/exposure time	30 min	6 min	16.7 min (1000 s)
Occupational exposure	$50\,\mathrm{W\,m^{-2}}$	$100\,\mathrm{W\,m^{-2}}$	$100\,\mathrm{W\,m^{-2}}$
Public exposure	$10\,\mathrm{W\,m^{-2}}$	$50\,\mathrm{W\,m^{-2}}$	

There are different assumptions in the ICNIRP guidelines for RF-EMF up to 300 GHz and Incoherent infrared. Also, the IR guidelines are poorly treated for the longest wavelength (Far IR or IR-C) above 3 µm. The assumed

limit for IR-C is in the same order as RF-EMF occupational exposure at 300 GHz, but that does not mean it can be compared directly.

[18] specifies the exposure limit of laser radiation within the wavelength range from 180 nm to 1 mm. The exposure limits for the eye and the skin as defined in [18] are summarized in Table 7. For eye exposure, all limits are defined at the corneal plane, oriented perpendicular to the optical axis of the eye. For skin exposure, the same numerical limit values apply, however, they are specified with respect to a limiting aperture of 3.5 mm.

Table 7: Exposure limits for the eye, specified as radiant exposure at the cornea and expressed as either radiant power or radiant energy transmitted through a 7 mm aperture. The same exposure limits apply to the skin, with the exposure limits specified at the skin surface and a 3.5 mm aperture.

Wavelength (nm)	Exposure duration		Exposure limit ($W\,m^{-2}$ or $J\,m^{-2}$)
	Lower limit	Upper limit	
2600 nm $\leq \lambda <$ 1 mm	1 ns	100 ns	$100\,J\,m^{-2}$
2600 nm $\leq \lambda <$ 1 mm	100 ns	10 s	$5.6\,t^{0.25}\,kJ\,m^{-2}$
1400 nm $\leq \lambda <$ 1 mm	10 s	30 ks ($\sim$8 h)	$1.0\,kW\,m^{-2}$

3 Measuring and assessing EMF

3.1 Standards and recommendations: ITU and ICNIRP

A number of well-established recommendations provide a solid “toolbox” for RF-EMF compliance work. In our review they can be positioned as the normative backbone that defines what to assess, how to assess it, and how to document/communicate compliance.

At the top level, ITU-T K.91 [5] is an umbrella document, that consolidates guidance for assessment, evaluation, and monitoring of human exposure in real environments with potentially multiple RF sources over frequency range from 8.3 kHz up to 300 GHz and it explicitly links exposure evaluation to existing standards and procedures.

Building on that, ITU-T K.52 [4] provides the general compliance logic (limits framework, multi-source principles, assessment flow, and practical evaluation techniques), which is helpful as the “entry point” to decide whether a scenario needs detailed analysis and what method class (calculation/measurement) is appropriate.

ITU-T K.61 [20] provides practical guidance on measurement and numerical prediction methods for demonstrating compliance with human exposure limits for telecommunication installations. In this sense, it acts as the methodological “how-to” companion to K.91 and K.52, giving concrete guidance on the selection of measurement quantities, probe and instrument choice, uncertainty handling, averaging procedures, treatment of multiple sources, and the use of numerical techniques when measurements are difficult or not sufficiently reliable, especially in complex or near-field situations. This makes it particularly relevant when justifying the choice between measurement-based and simulation-based assessment methods.

ITU-T K.122 [21] focuses on expected exposure levels in close proximity to radiocommunication antennas and is therefore particularly relevant for occupational scenarios such as installation and maintenance. It provides representative full-wave simulation results for typical antenna configurations and shows how these results can be rescaled for different transmitter powers and simultaneous emissions. In this way, it serves as a practical reference for understanding likely near-antenna exposure conditions and for identifying cases where more detailed case-specific analysis or control measurements are needed.

The ICNIRP Guidelines on Limits of Exposure to Laser Radiation [18] provide exposure limits to laser radiation in the wavelength range from 180 nm to 1000 µm. The document aims to prevent adverse biological effects on human eyes and skin. Although primarily developed for laser radiation safety, these guidelines can be used as a reference for EMF exposure above 300 GHz, where dedicated exposure standards are still limited. Its appendix gives a pragmatic overview of which numerical technique fits which scenario (e.g., FDTD/MoM for near-field or complex scattering, ray tracing for far-field multi-scatter environments, and hybrid approaches), making it a clean reference to justify the modelling choice in your methodology section.

3.2 EMF basic measurements and assessment flow

Two main approaches can be used for RF EMF exposure assessment: measurement-based and calculation-based. The choice between them depends on the practical situation: measurements are typically preferable for existing installations when transmitter parameters are incomplete or uncertain, whereas calculations are essential for planning and design of new or modified installations and can also complement measurements when only partial site information is available. A structured assessment workflow is provided in Recommendation ITU-T K.91 [5].

3.2.1 Measurement-based assessment

Measurements are particularly suitable for existing installations and real environments where many emitters operate simultaneously, especially when complete transmitter or antenna information is unavailable. Measure-

ments can be performed without complete knowledge of all radiating sources, provided that suitable equipment is available and at least the relevant frequency range is known. Nevertheless, source information improves the accuracy and reliability of the assessment. Useful information includes: 1) operating frequency, to ensure probe coverage; 2) distance to the transmitting antenna, to determine the field region; 3) maximum equivalent radiated power (ERP), to estimate expected levels and instrument dynamic range; 4) whether antennas operate at maximum transmitter (Tx) power during the measurements; and 5) modulation characteristics.

Broadband RF EMF measurements are assumed to be used as the first step in the assessment flow. Since the broadband result is usually evaluated against the most restrictive reference level within the instrument's frequency range, the outcome is generally conservative. Consequently, if compliance is demonstrated using broadband measurements, additional measurements are typically not required.

If broadband results are close to the limits or indicate non-compliance, frequency-selective measurements should be used to separate and quantify contributions from individual services/bands. This allows the exposure ratio to be calculated for each relevant frequency component and then combined to obtain the total exposure. Frequency-selective assessment requires post-processing to integrate contributions per signal band and apply the appropriate reference levels. Post-processing is also required when broadband measurements must use more than one probe/antenna to cover all operating emissions. If frequency-selective results still suggest a possible exceedance, the assessment should be refined using methods linked to basic restrictions (e.g., SAR-based approaches).

The equipment should indicate root mean square (RMS) values as per ICNIRP/IEEE practice (unless national rules specify otherwise). For frequency-selective measurements, resolution bandwidth (RBW) strongly affects results for broadband/modulated signals.

In the far field, measuring orthogonal E-field components is generally sufficient. In the reactive near field, however, the measurement problem is much more complex: both E- and H-field components should be measured and, in principle, three orthogonal components of each quantity are required.

For low-THz frequencies, measurement-based assessment becomes strongly limited by instrumentation. A key difficulty is the probe-size requirement in the near field: the characteristic sensor dimension should be smaller than one wavelength at the highest operating frequency [20]. At 300 GHz, this corresponds to about 1 mm. Such a constraint makes the realization of isotropic, calibrated, low-perturbation probes extremely difficult, particularly for reactive near-field measurements where both E and H are needed. As a consequence, near-field measurements above 100 GHz are of very limited practical feasibility and, for many realistic compliance scenarios, are close to impractical with currently available commercial probe technology.

This practical limitation is also reflected by the current market situation. Commercial broadband/isotropic EMF probes are readily available up to about 90 GHz for electric-field measurements, while dedicated magnetic-field probes are available only over much lower frequency ranges. In other words, no widely marketed isotropic probes for EMF compliance measurements appear to be available in the low-THz range. Therefore, a purely measurement-based compliance assessment with conventional field probes is generally not realistic for reactive near-field exposure at frequencies around 100 GHz and above.

For radiating far-field conditions, the situation is more favorable. Frequency-selective measurements can still be performed using a calibrated receiving antenna or horn together with a spectrum analyser or signal analyser and, where necessary, an external frequency converter or harmonic mixer. In such a setup, the received signal is converted into electric-field strength by means of the antenna factor [20].

3.2.2 Calculation-based assessment

Calculations are essential when new RF sources are planned, because compliance must be demonstrated for configurations that do not yet exist in operation. In such cases, assessment is performed by calculation or by a combination of measurement and calculation (e.g., measure the existing environment and add calculated contributions from the planned equipment).

In contrast to measurements, calculation always require information about the radiating sources and achievable accuracy depends strongly on the level of detail available.

In [5], a hierarchy of models with increasing accuracy and data requirements is presented: (1) a single point-source model, requiring only the operating frequency, distance, and maximum equivalent isotropically radiated power (EIRP); (2) a synthetic model for antenna systems with many elements (e.g., panels/patches), which requires antenna geometry and details of the feeding arrangement; and (3) full-wave methods such as method of moments (MoM) and finite difference time domain (FDTD), which are used for the most accurate predictions and for near-field cases, but require a high level of detail in the input data, as well as specialized software, expertise, and significant computational resources.

3.2.3 Calculation-based assessment for RIS-assisted channels

Reconfigurable intelligent surfaces (RISs) are frequently proposed as an enabling technology for low THz indoor/industrial channels, where strong path loss and blockage motivate the use of highly directive beams and controllable reflections. In the context of RF EMF assessment, two RIS cases could be distinguished.

Active RIS: if the RIS is actively fed or can be represented as a set of radiating elements with known delivered powers, it can be treated analogously to an antenna array and assessed using the synthetic model in [5], where the radiating structure is represented by many elementary sources (patches/panels) and the total field is obtained by their superposition. The applicability of this model is discussed beyond a near-field distance defined with respect to the maximum size of a radiating source, rather than the size of the entire aperture. However, for low THz RIS implementations the number of elements is typically very large (element size scales with wavelength), and the feeding phases required by the synthetic model become difficult to obtain in practice. A conservative adaptation can be formed by considering the worst-case coherent addition at the point of investigation (POI). Then synthetic model electric field strength:

$$E = \sum_n \frac{\sqrt{30\, P_n\, G_n}}{r_n} \exp\left[j\left(\gamma_n + \frac{2\pi r_n}{\lambda}\right)\right] \tag{3}$$

becomes

$$E = \sum_n \frac{\sqrt{30\, P_n\, G_n}}{r_n} \tag{4}$$

where E is the complex electric-field strength at the POI, P_n is the power delivered to the n-th elementary radiator, G_n is the gain of the n-th radiator in the direction of the POI, r_n is the distance from the n-th radiator to the POI, γ_n is the relative phase of the excitation (feed phase) of the n-th radiator, λ is the wavelength. The term $2\pi r_n/\lambda$ represents the propagation phase from the n-th radiator to the POI.

Passive RIS: if the RIS is not actively powered and mainly acts as a reflecting/scattering structure, it can be treated as an additional reflecting object that may increase the field level at the POI. The influence of reflections is conservatively accounted for by multiplying the calculated electric field strength by a multipath component (MPC) factor. In complex environments with multiple reflections, use of the highest multiplication factor is recommended. The maximum multiplication factor is 2 for the electric field strength (corresponding to 4 for power density) [5].

3.3 The near-field problem

The near-field region is located in proximity of an antenna or another radiating element. Within the near-field, electromagnetic waves do not exhibit a plane-wave behavior. The boundaries of the field regions depend on

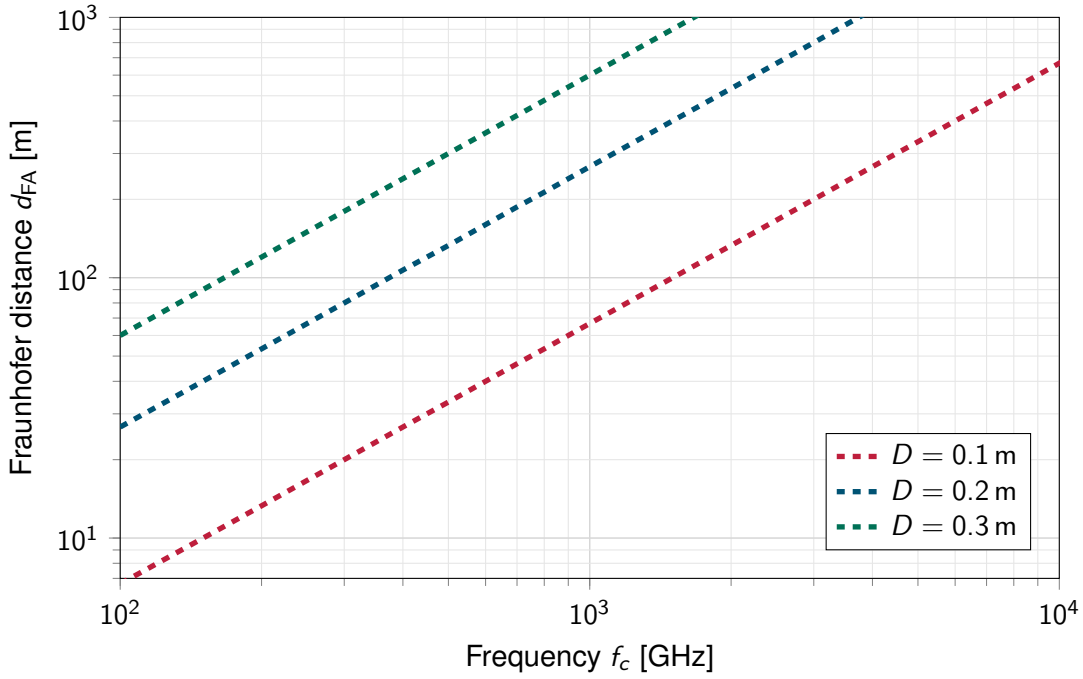

Figure 4: Fraunhofer distance as a function of the carrier frequency over the THz band.

the antenna dimension D and the wavelength λ. Fraunhofer distance $d_{\text{Fraunhofer}}$ defines the beginning of the far-field region:

$$d_{\text{Fraunhofer}} = \frac{2D^2}{\lambda} . \tag{5}$$

In the reactive near-field region, the amplitude and phase of the E- and magnetic H-fields vary strongly with position. Additionally, energy is predominantly stored rather than radiated, and therefore does not propagate away from the antenna [5].

Workers are more likely to stay close to RF sources compared with the general public. In some cases, the designated working area is located within the reactive near-field region, which necessitates the use of more advanced and rigorous exposure assessment methodologies due to the increased field complexity. At higher operating frequencies, the spatial extent of the reactive near-field region increases as can be seen in (5). Consequently, near-field exposure limits relevant to the general public also become important considerations in the overall compliance assessment [5].

TIMES Deliverable 4.1 [22] states that for THz frequencies range in the industrial environment scenarios, that are the scenarios of interest in the TIMES project, communication links are often located in the near-field region.

Figure 4 [22] illustrates how the Fraunhofer distance depends on frequency and on the physical dimension of an antenna (or antenna array). For a frequency of 300 GHz and an antenna aperture of 0.1 m, the far-field boundary is approximately 20 m. In industrial indoor scenarios, high-aperture arrays and reconfigurable intelligent surfaces (RIS) are often required. Since typical link distances are on the order of tens of meters (and rarely hundreds of meters or more), communication frequently occurs within or close to the near-field region.

The scenario under investigation in D4.1 considers a carrier frequency 300 GHz, square patch antennas with the dimension of $318\sqrt{2}\lambda \sim 45$ cm and correspondingly $d_{\text{FA}} \sim 404$ m. The considered industrial scenario has a coverage area with a squared cell of side length L. Two cases were considered: $L = 20$ m (corresponding to a

small-scale scenario) and $L = 50\,\mathrm{m}$ (corresponding to a large-scale scenario). That gives a communications links operating purely in the near-field region.

The other important aspect stated by the [22] is that near-field propagation enables beamfocusing, i.e., beamforming with depth (range) selectivity, since the impinging wavefronts across a large array are spherical and retain noticeable curvature over the array aperture. This curvature makes the array response depend on both direction and distance, so users can, in principle, be separated not only by angle but also in the depth domain. In contrast, in the far-field the wavefronts are approximately planar, and the array response depends mainly on direction; hence, conventional beam steering can separate users by angle, but range-based focusing (depth separation) is no possible.

Overall, reliable investigation and assessment of EMF exposure levels in realistic near-field conditions becomes essential for THz industrial scenarios. This motivates dedicated measurement and evaluation procedures that explicitly account for near-field propagation and beamfocusing behavior at THz frequencies.

3.3.1 Basic restrictions

For the radiative near-field, the reference levels from Table 3 and 4 can be applied. However, in the reactive near-field these values cannot be used; therefore, the basic restrictions must be considered.

The basic restrictions from Table 2 apply in the near-field because they are based on physical quantities inside the human body and are therefore independent of the field region.

3.3.2 Reference levels

Table 3 specifies the reference levels for frequencies from 400 MHz to 300 GHz, averaged over the whole body and a time interval of 30 min.

In the radiative near-field region, compliance for frequencies from 400 MHz to 2 GHz is achieved if either the incident power density S_{inc} does not exceed the applicable reference level, or both the incident electric field strength E_{inc} and the incident magnetic field strength H_{inc} remain below their respective reference levels, evaluated under the same averaging and exposure conditions as defined for the far-field region.

For frequencies from 2 GHz to 300 GHz, compliance is demonstrated if the incident power density S_{inc} does not exceed the corresponding reference level specified for S_{inc}.

For Table 4, which specifies the ICNIRP (2020) reference levels for local exposure from 400 MHz to 300 GHz averaged over 6 min, compliance in the radiative near-field region is assessed under the same conditions as defined for the far-field region. For frequencies from 30 MHz to 6 GHz, compliance is achieved if either the peak spatially averaged incident power density, S_{inc}, does not exceed the applicable reference level, or both the peak spatially averaged incident electric field strength, E_{inc}, and magnetic field strength, H_{inc}, remain below their respective reference levels.

For the frequency range from 6 GHz to 300 GHz, the same general conditions apply for the radiative near-field, however, compliance is demonstrated solely by verifying that the peak spatially averaged incident power density, S_{inc}, does not exceed the applicable reference level.

The reactive near-field region cannot be assessed using the reference levels specified in Tables 3 and 4, as these quantities are derived under plane-wave assumptions that are generally not fulfilled in this region. Instead, compliance evaluation must be based on the corresponding basic restrictions defined in Table 2.

3.3.3 Full-Wave Models

The highest accuracy for calculating the reference levels can be achieved using numerical modeling. Numerical modeling can be performed using full-wave methods, which are based on solving Maxwell's equations in the

time or frequency domain [5].

Models that can be used here include the Method of Moments (MoM) or the Finite Difference Time Domain Method (FDTD).

MoM is used to solve electromagnetic integral equations in the frequency domain. It is especially useful for problems involving electromagnetic sources, such as radiation and scattering. The method can be applied to both boundary and volume integral equations [23].

The FDTD method is used to solve Maxwell's equations in the time domain. The simulation region is divided into many small grid cells, and the electric and magnetic fields are calculated alternately over time [23].

These models can be used for all source regions. However, they require appropriate software, expertise in electromagnetics, substantial computer resources, and very detailed input data. The results depend strongly on the input data that are provided.

Full-wave models make it possible to consider all important factors that influence radiation. Nevertheless, they are typically only used in simple scenarios or in the reactive near field, where other methods fail or are not sufficiently accurate, as it is very difficult to collect all the required data.

3.4 Influence of the MPCs

In indoor low THz and THz channels, the EMF distribution is strongly influenced by the surrounding environment. In contrast to free-space conditions, industrial and indoor environments contain walls, metallic structures, machines, floors, ceilings, and other objects that generate reflected and scattered field components. As a result, the total field at a given observation point is not determined only by the direct path from the Tx, but by the superposition of MPCs. This effect is especially relevant in complex environments and in the near-field region, where the field does not exhibit a simple plane-wave behaviour and may vary significantly from point to point [5], [21].

From the EMF assessment perspective, these reflected and scattered components can locally increase the electric field strength and power density compared to the free space prediction. [5] explicitly notes that reflections from the ground and from surrounding structures such as buildings, fences, and metallic objects may increase the field level, and therefore should be taken into account in conservative compliance assessments. Full-wave numerical methods, such as the MoM, are able to include such objects as secondary sources causing reflections, but their use requires detailed geometric and electromagnetic input data and is often limited to relatively simple configurations or near-field studies.

For practical compliance evaluations, the influence of the environment is often introduced through a conservative multiplication factor. For observation points located a few meters above the terrain, ground reflections may be represented by multiplying the electric field strength by 1.6, corresponding to a power-density factor of 2.56. In more complex environments with multiple reflections, the highest applicable multiplication factor should be used; in practice, the maximum factor is 2 for electric field strength, corresponding to 4 for power density. This approach provides a simplified but conservative way to account for MPC-related field enhancement when a detailed site-specific electromagnetic simulation is not available [5].

Report [24] highlights that channels above 100 GHz are typically sparse, with propagation dominated by a limited set of significant reflected paths, while scattering and blockage effects become stronger as frequency increases. Therefore, even though the number of dominant MPCs may be limited, their contribution can be significant for both communication performance and local EMF distribution.

Consequently, assessment of EMF exposure in complex indoor environments should not rely solely on idealized free-space assumptions. The impact of reflections, scattering, and other environment-dependent MPCs should be considered either by detailed numerical modelling or, where this is not feasible, by applying conservative multiplication factors. This ensures that local field enhancements caused by the indoor environment are not underestimated in the compliance analysis.

4 Analysis of TIMES scenarios

4.1 General analysis of scenarios matrix

The TIMES scenarios were originally defined to cover the main classes of industrial THz communication conditions relevant for the project, including intra- and inter-device links, static and dynamic situations, scenarios with moving objects or moving Tx/Rx, and cases involving RIS [25]. Table 8 summarizes the overall logic of the scenarios definition.

Table 8: Channel measurement scenario matrix [25]

Type	**Intra-device scenarios**	**Inter-device scenarios**
Device type	Medium and Large	Medium and Large
Static	Yes	Yes
Mobile scenario, moving Tx or Rx	No	Yes
Mobile scenario, moving object	Yes	Yes
Includes RIS	Yes	Yes
ISAC relevant	Yes	Yes
EMF relevant	Yes	Yes
Environment, e.g., air quality	Clean/Dusty/Humid...	Clean/Dusty/Humid...

For EMF exposure analysis, the scenarios should not only be grouped by communication type, but also by the properties that determine how difficult or critical exposure evaluation is in practice. The relevant aspects are: 1) whether workers can access the vicinity of the radiating equipment; 2) whether the link is likely to operate in the reactive near-field, radiative near-field, or far-field; 3) whether the environment is static or time-varying; 4) the expected richness of MPC; 5) whether the scenario is more suitable for measurement-based or calculation-based. This is consistent with the general assessment logic already discussed in Section 3, where the choice of method depends strongly on source information, field region, and scenario complexity.

A first important distinction is between intra-device and inter-device scenarios. Intra-device scenarios are particularly relevant for EMF analysis because they represent confined environments with short Tx–Rx distances and complex surrounding structures. In the TIMES scenario list, these cases mainly correspond to intra-machine links with distances of 10 cm–100 cm. Such short distances, especially in combination with large apertures at THz frequencies, are highly relevant for near-field exposure conditions, as discussed in Section 3.3. In addition, the scenario definition explicitly notes that workers may be located inside machines during maintenance or repair. Furthermore, measurements performed within the TIMES project in intra-machine scenarios indicated a strong presence of MPCs [26], [27]. This suggests that the conservative assessment approaches, for example by introducing an MPC-related multiplication factor or, where necessary, more advanced full-wave methods, may be required.

By contrast, inter-device scenarios generally represent larger factory-floor links, typically over distances of tens of meters, between access points, machines, sensors, robots, or operators. These scenarios are usually more open geometrically, but they remain highly relevant for EMF assessment because a worker or mobile robot may cross the main beam or a reflected propagation path. In addition, such scenarios can involve non-line-of-sight (NLoS) conditions, moving objects, mobile terminals, and RIS-assisted links, all of which can change the spatial distribution of the field and therefore the location of exposure maxima.

A second important distinction is static versus dynamic exposure conditions. Static scenarios are the most straightforward from an assessment perspective, since the field distribution can be characterized for a fixed geometry using measurements, deterministic calculations, or a combination of both. Dynamic scenarios are more challenging. When the environment contains moving objects, the field distribution may change over time

due to blockage, reflection, diffraction, or scattering. When Tx or receiver (Rx) itself moves, the entire exposure zone may become position-dependent and time-varying. Therefore, dynamic scenarios are not necessarily associated with higher average exposure, but they are associated with higher assessment complexity because a single static measurement point may not be representative.

A third key aspect is the propagation condition: line-of-sight (LoS) scenarios may create more direct and spatially concentrated exposure regions, while NLoS scenarios may reduce direct illumination but can still produce local maxima due to strong reflections or redirection of power. This is particularly relevant in industrial environments with metallic machinery and structured surroundings, where multipath propagation is strong. The same issue becomes even more important when RIS is present, since the surface is intentionally introduced to reshape the spatial propagation channel. In communication terms this is beneficial, but in EMF terms it means that not only the direct path, but also the redirected energy paths should be considered when evaluating local exposure. A more detailed assessment of RIS-assisted channels is provided in Section 3.2.3 of this report.

Based on these observations, the main EMF relevance of the TIMES scenarios is not identical across all cases. The intra-device short-range scenarios are the most critical with respect to near-field assessment as well as for the MPCs influence and possible use of more advanced methods, including full-wave modelling in the most demanding cases. Static inter-device scenarios are generally easier to survey but may still require careful treatment of beam directionality and worker accessibility. Dynamic inter-device scenarios, especially those involving moving Tx or Rx, are important because exposure maxima may shift over time and because compliance demonstration may need to rely more strongly on calculation-based or hybrid approaches than on measurements alone. RIS-assisted scenarios form a separate class because they combine high directive operation with intentional redirection of energy and therefore deserve dedicated treatment in any conservative EMF analysis.

Overall, the TIMES scenario set covers the main industrial conditions that are relevant for future THz EMF assessment. At the same time, the analysis indicates that the most challenging cases from the compliance perspective are not simply “all THz scenarios”, but specifically those that combine short distances, worker accessibility, complex multipath, mobility, and RIS-assisted propagation. These are the cases where simplified far-field assumptions are least reliable and where refined modeling or hybrid assessment procedures are most likely to be needed.

Table 9 summarizes the TIMES scenario types from the perspective of EMF exposure assessment, highlighting the main EMF-related concerns and the corresponding suitable assessment methods based on [20] and [5].

Table 9: EMF-oriented classification of TIMES scenarios

Scenario	Distance	Field region	Main EMF concern	Calculation	Measurement
Intra-device scenarios					
Large machine, static	1–10 m	Mainly near-field; far-field possible for small apertures	Worker proximity, MPCs, local hot spots	FDTD, MoM	Far-field feasible; near-field of very limited feasibility*
Large machine, moving object	1–10 m		Time-varying exposure, changing MPCs	FDTD, MoM (snapshots)	Far-field feasible; required time/spatial averaging; near-field of very limited feasibility*
Large machine, RIS inside	1–10 m		RIS-induced energy concentration	FDTD, MoM	Far-field feasible; near-field of very limited feasibility*
Medium machine, static	10 cm–100 cm	Very likely near-field	Short range, reactive near-field, MPCs	FDTD, MoM	Of very limited feasibility*
Medium machine, moving object	10 cm–100 cm		Time-varying short-range exposure	FDTD, MoM (snapshots)	Of very limited feasibility*
Inter-device scenarios					
Medium machine, static	10–100 m	Near-/far-field depends on aperture	Exposure in work areas	Ray tracing, MoM	Far-field E-field measurement feasible
Medium machine, moving object	10–100 m		Time-varying exposure, blockage, reflections	Ray tracing	Far-field E-field measurement feasible; required time/spatial averaging
Medium machine, moving Tx/Rx	10–100 m		Moving exposure zone	Ray tracing	Far-field E-field measurement feasible; required time/spatial averaging
Medium machine, static, RIS-assisted	10–100 m		RIS-induced redistribution, local maxima	Ray tracing, MoM	Far-field E-field measurement feasible

*No practical equipment for separate E- and H-field measurements in the low-THz/THz near field was identified.

4.2 TIMES PoCs analysis

As described earlier in this document, two PoCs were implemented within the TIMES project using hardware developed in TIMES to demonstrate the practical feasibility of THz links in realistic industrial environments.

Below, an EMF safety assessment of these two demonstrations is provided

According to [4], the first step is to check the EIRP of the transmitting source. If the maximum EIRP is lower than 2 W, the source can be classified as inherently compliant and no further assessment is required. In the case of PoC1, the EIRP was in the range of 41 dBm to 43 dBm, which corresponds to approximately 12.6 W to

20 W. Therefore, further assessment of this scenario is required.

For PoC2, the EIRP was 25 dBm in the case of PoC2.1 with the horn-lens antennas and 2 dBm in the case of PoC2.2 with the LWA. These values correspond to approximately 0.32 W and 1.6 mW, respectively. Since both values are below the 2 W threshold, the transmitting source in PoC2 can be considered inherently compliant and no further assessment is required.

Since the EIRP of PoC1 exceeds 2 W, a more detailed assessment is required. The next step is therefore to estimate the minimum distance that must be kept from the antenna based on equation 6 [28].

$$S = \frac{\text{EIRP}}{4\pi d^2} \tag{6}$$

$$d_{\text{min}} = \sqrt{\frac{\text{EIRP}}{4\pi S_{\text{max}}}} \tag{7}$$

here S is the incident power density (W/m^2) and d is the distance from the antenna (m).

Based on the ICNIRP guidelines, as summarized in [5], the whole-body reference level for general public exposure in the frequency range from 2 GHz to 300 GHz is $S = 10\,\text{W/m}^2$. Using equations 6 and 7, this yields a minimum accessible distance of 0.32 m for an EIRP of 41 dBm and 0.40 m for an EIRP of 43 dBm. However, these values should only be regarded as a first far-field screening estimate.

According to [28], the simplified relation used in equations 6 and 7 is generally applicable only under far-field conditions. Therefore, the near-field/far-field boundary must first be estimated for the considered demonstrator. The high-gain lens antennas considered here have a diameter of 226 mm. At 300 GHz, this results in a Fraunhofer distance of approximately 102 m. Using the conservative K.100-style approach, the boundary of the reactive near-field region can be estimated as $\max(\lambda, D, D^2/(4\lambda))$, which gives approximately 12.7 m. Consequently, the distance of 0.40 m obtained from the simplified far-field equation lies deep inside the reactive near-field region and therefore cannot be considered a valid compliance distance. Even if the less conservative antenna-theory expression $0.62\sqrt{D^3/\lambda}$ is used, the corresponding reactive near-field boundary is still approximately 2 m, which likewise shows that the calculated minimum distance lies inside the reactive near-field region.

It is worth noting that the paper [29] shows that, for a specific passive RIS channel scenario at 300 GHz, the bistatic radar equation can provide good path-gain agreement down to approximately one tenth of the Fraunhofer distance. In the present case, one tenth of the Fraunhofer distance corresponds to approximately 10.2 m, that aligned well with the conservative ITU approach for the reactive near-field estimation with 12.7 m boundary. This observation supports the general statement that the transition between near field and far field can be physically smooth, rather than being characterized by a strict boundary and motivate further investigation of whether the far-field approach of equation 6 could remain useful in part of the radiating near-field region.

For the present case, near-field assessment should instead be based on the evaluation of the electric field or power density at all relevant accessible points, followed by comparison of the maximum value with the applicable exposure limit. In principle, this can be done either by measurements or by numerical modelling. However, due to the equipment limitations discussed above, a measurement-based assessment is highly challenging at these frequencies. Therefore, the most realistic and defensible approach for the present case would be the use of full-wave numerical methods.

5 Conclusions

This report reviewed the current state of EMF exposure assessment for low-THz and THz systems, with particular focus on the industrial scenarios considered in the TIMES project. The analysis shows that the established RF EMF compliance framework remains well defined up to 300 GHz, while for frequencies above 300 GHz the assessment basis is less mature and requires careful interpretation of the available guidance.

This deliverable shows that THz industrial scenarios cannot be assessed reliably using a single generic approach. The choice of method depends strongly on the field region, source configuration, environmental complexity, and the availability of transmitter and antenna data. For far-field conditions, measurement-based assessment remains feasible and can be supported by conventional frequency-selective methods using calibrated receiving antennas and suitable converters. In contrast, reactive near-field assessment at low-THz frequencies is a major challenge, since it requires separate evaluation of electric and magnetic field components, while practical probe technology for routine isotropic near-field measurements above about 100 GHz is very limited. As a result, purely measurement-based compliance assessment is generally not realistic for many short-range THz scenarios.

The report further shows that near-field conditions are expected to be common in THz industrial deployments, particularly for short links and large apertures. In such cases, simplified plane-wave assumptions are not generally valid, and compliance evaluation may need to rely on basic restrictions and advanced numerical methods. Full-wave methods therefore become important tools for the most demanding cases, despite their high requirements in terms of model detail, computational resources, and expertise.

Another key result is the importance of the propagation environment. In realistic indoor industrial settings, reflections, scattering, blockage, and RIS-assisted redirection can significantly modify the spatial EMF distribution and create local field maxima. Therefore, EMF assessment should not rely only on free-space assumptions. Depending on the scenario, this influence should be treated either by detailed modeling or by conservative multiplication factors when a full site-specific analysis is not feasible.

From the TIMES perspective, the most critical scenarios are the intra-device and short-range cases, especially those combining worker accessibility, near-field operation, strong multipath, mobility, and RIS-assisted propagation. By contrast, larger inter-device scenarios are generally more amenable to far-field measurements, although dynamic operation and redirected propagation paths still increase assessment complexity. Overall, the report indicates that future THz EMF compliance in industrial environments will require scenario-dependent assessment strategies and further methodological development for realistic near-field conditions.

References

[1] Guidelines for Limiting Exposure to Electromagnetic Fields (100 kHz to 300 GHz). Health physics, 118(5):483–524, 2020.

[2] Smart Networks and Services Joint Undertaking. SNS R&I Work Programme 2021–2022.

[3] 5G PPP TMV WG/ EMF TF. Whitepaper: Beyond 5G/6G EMF Considerations. 2023.

[4] ITU-T K.52 (08/2024) - Guidance on complying with limits for human exposure to electromagnetic fields.

[5] ITU-T K.91 (01/2024) - Guidance for assessment, evaluation and monitoring of human exposure to radio frequency electromagnetic fields.

[6] IEEE Standard for High Data Rate Wireless Multi-Media Networks–Amendment 2: 100 Gb/s Wireless Switched Point-to-Point Physical Layer.

[7] Demos Serghiou, Mohsen Khalily, Tim W. C. Brown, and Rahim Tafazolli. Terahertz Channel Propagation Phenomena, Measurement Techniques and Modeling for 6G Wireless Communication Applications: A Survey, Open Challenges and Future Research Directions. IEEE Access.

[8] X. Qi, K. Bertling, J. Torniainen, F. Kong, T. Gillespie, C. Primiero, M. S. Stark, P. Dean, D. Indjin, L. H. Li, E. H. Linfield, A. G. Davies, M. Brünig, T. Mills, C. Rosendahl, H. P. Soyer, and A. D. Rakić. Terahertz in vivo imaging of human skin: Toward detection of abnormal skin pathologies. APL bioengineering, 8(1):016117, 2024.

[9] Lulu Wang. Terahertz imaging for breast cancer detection. Sensors (Basel, Switzerland), 21(19), 2021.

[10] Seung Jae Oh, Sang-Hoon Kim, Young Bin Ji, Kiyoung Jeong, Yeonji Park, Jaemoon Yang, Dong Woo Park, Sam Kyu Noh, Seok-Gu Kang, Yong-Min Huh, Joo-Hiuk Son, and Jin-Suck Suh. Study of freshly excised brain tissues using terahertz imaging. Biomedical optics express, 5(8):2837–2842, 2014.

[11] Xurong Li, Jingxi Li, Yuhang Li, Aydogan Ozcan, and Mona Jarrahi. High-throughput terahertz imaging: progress and challenges. Light, science & applications, 12(1):233, 2023.

[12] IEEE International Committee on Electromagnetic Safety. C95.1-2019 - IEEE Standard for Safety Levels with Respect to Human Exposure to Electric, Magnetic, and Electromagnetic Fields, 0 Hz to 300 GHz. IEEE, 2019.

[13] Federal Communications Commission. 47 CFR § 1.1310 Radiofrequency radiation exposure limits.

[14] GSMA. EMF Policy. https://www.gsma.com/solutions-and-impact/connectivity-for-good/public-policy/regulatory-environment/emf-and-health/emf-policy/. Accessed: 2026-03-04.

[15] GSMA. International EMF Exposure Guidelines: Explaining the 2020 RF-EMF exposure guidelines published by the International Commission on Non-Ionizing Radiation Protection (ICNIRP) Exposure Guidelines Explaining the 2020 RF-EMF exposure guidelines published by the International Commission on Non-Ionizing Radiation Protection (ICNIRP). 2021.

[16] ISO. Optics and Photonics - Spectral bands (ISO 20473:2007).

[17] ICNIRP. Guidelines on Limits of Exposure to Incoherent Visible and Infrared Radiation. Health physics, 105(1):74–96, 2013.

[18] ICNIRP Guidelines on Limits of Exposure to Laser Radiation of Wavelengths between 180 nm and 1,000 um. Health physics, 105(3):271–295, 2013.

[19] ICNIRP. Statement on Far Infrared Radiation Exposure. Health physics 91(6):630–645, 2006.

[20] ITU-T K.61 (10/2025) - Guidance on measurement and numerical prediction of electromagnetic fields for compliance with human exposure limits for telecommunication installations.

[21] ITU-T K.122 (12/2016) - Exposure levels in close proximity of radiocommunication antennas.

[22] SNS TIMES. D4.1: Intermediate report on PHY layer enhancements for THz links supporting sensing and communication functionalities. 2023.

[23] Walton C. Gibson. The Method of Moments in Electromagnetics. Chapman & Hall/CRC, Boca Raton, FL, 2008.

[24] ITU-R M.2541-0 (05/2024) - Technical feasibility of IMT in bands above 100 GHz.

[25] SNS TIMES. D2.1: Definition of use cases, KPIs, and scenarios for channel measurements. 2023.

[26] SNS TIMES. D3.1: Initial channel measurements in industrial environments as sub-THz frequencies. 2023.

[27] SNS TIMES. D3.2: Channel Measurements in industrial setting with IRS at sub-THz frequencies. 2025.

[28] ITU-T K.100 (08/2024) - Measurement of radio frequency electromagnetic fields to determine compliance with human exposure limits when a base station is put into operation.

[29] Lorenz H. W. Loeser, Sérgio Matos, and Thomas Kürner. Channel Measurements Involving Passive RIS at 300 GHz. 2025 19th European Conference on Antennas and Propagation (EuCAP), 2025.